

*x-ray and neutron*

# **CRYSTALLOGRAPHY**

*a powerful combination*  
by Robert B. Von Dreele

**D**etermining the structure of a crystalline material remains the most powerful way to understand that material's properties—which may explain why so many Nobel Prizes have been awarded in the field of crystallography. The standard tools of the crystallographer are single-crystal and powder diffraction. introduced earlier in "Neutron Scattering-A Primer." What was not mentioned was that until twenty years ago powder diffraction could not be used for solving a new crystal structure, but only for determining the presence of known crystalline phases in powders of unknown composition. At that time material had to be grown into large single crystals before crystallographers could unravel the positions of each atom within the repeating motif of a crystal lattice. This severe limitation disappeared after H. M. Rietveld developed a workable approach for resolving the ambiguities of most powder-diffraction patterns. The technique, known as Rietveld refinement, has opened up essentially all crystalline materials to relatively rapid structure analysis.

This Escher painting shows a square lattice with a complicated unit cell, illustrating in two dimensions several kinds of symmetries found in real crystals. (We have darkened lines of the original grid to emphasize the unit cell.) If the colors are ignored, this pattern has both fourfold and twofold rotational symmetry as well as a number of mirror symmetry operations. When the color is included, the fourfold rotation becomes a color-transformation operator. Similar changes occur in the nature of the other symmetry operators as well. Reproduced with permission: © 1990 M. C. Escher Heirs/Cordon Art, Baarn, Holland.

This article presents a further improvement in powder-pattern analysis—that of combining x-ray and neutron diffraction data. We used this combination to make the first unambiguous determination of the structures of certain high-temperature superconductors and have since produced a portable software package for use by all crystallographers who collect both x-ray and neutron data. Here we will discuss the concepts and techniques that make the combination so useful and some of our recent results, including the determination of fractional occupancies by different elements at single atomic sites in a crystal. First, however, we need to extend the concepts on diffraction introduced in the primer.

## What Is a Crystal?

Most solids are crystals: They consist of very many repetitions of a single motif or “unit cell,” of atoms. These repetitions occur at a regular array of points in three dimensions, a “lattice.” The opening illustration is a two-dimensional analogue of a crystal. The unit cell there is square, and contains several objects each arranged in a particular way relative to the others. One question about this pattern is how much information one needs in order to reproduce it. Clearly, one need only describe a single object (a fish), the set of rules for positioning it and the other objects in the unit cell (the fish of other colors), and the dimension of the unit cell itself. With only this information the entire pattern can be laid out to infinity. The classification of how the objects are positioned in the unit cell (in most crystals these positions are symmetrical) and of how the unit cells repeat is the mathematical theory of spatial symmetry, which is a branch of group theory (see the sidebar “Crystal Symmetry Groups”).

The crystallographer’s goal is to measure the lengths and angles of the edges of the unit cell (the “lattice parameters”) and, more important, the arrangement of the atoms within the unit cell. Many kinds of arrangements are possible, for example, the interlacing of long molecular chains in a crystallized protein, or the stacking of metal and oxygen atoms in a superconducting oxide, but in any crystal the arrangement is the same in every unit cell. Why should atoms and molecules form such orderly structures? A solid holds together because the atoms and molecules in it are attracted to each other. Thus the minimum-energy configuration of the solid occurs when its constituents are in as close contact as possible with their neighbors. This criterion is usually realized by a regular array, just as bricks in a neat stack are in closer contact and take up less space than bricks in a jumbled pile.

The unit cell of a crystal is extremely small, typically 10 angstroms ( $10^{-7}$  centimeter) on a side, whereas the sides of crystals in a powder may be 1000 to 100,000 times larger. An equivalent stack of bricks, each 20 centimeters on a side, would extend between 200 meters and 20 kilometers. The disparity in size between a unit cell and a crystal is so vast that we can model a crystal as if it contained an infinite number of unit cells in all directions. This approximation has an enormous simplifying effect on a mathematical description of a crystal because we need to describe only the unit cell and can ignore the crystal as a whole except to note that the unit cell repeats indefinitely in all directions.

With these ideas in mind, we can start with crystallographic mathematics and then connect it with the way a crystal scatters neutrons (reversing the plan of the primer). How do we mathematically describe a crystal? First, the description must reflect what we actually observe about a crystal. We “see” atoms in a crystal by scattering neutrons or x rays from them, so the mathematical model needs to describe the density of scattering power,  $p(\mathbf{r})$ , a function of position,  $\mathbf{r}$ , within the crystal. This scattering density is smooth and usually real and positive. (In some special cases it can be negative or even complex.) Second, the function needs to repeat infinitely in all directions to match the repetition of the unit cells. In one dimension  $p(x)$  might look like the curve in Fig. 1a, which gives the x-ray scattering density along one di-

rection in molybdenum disulfide for two unit-cell repeats. The tallest peaks represent the scattering density around the molybdenum atoms; the smaller peaks on either side correspond to the sulfur atoms. Like any periodic function, the variation of the scattering density with position  $x$  along the repeat direction can be expressed as an infinite sum of sine and cosine functions, or in other words, as a Fourier series in one dimension:

$$\begin{aligned}\rho(x) &= \frac{1}{a} \sum_{n=0}^{\infty} F_n \left[ \cos \left( -2\pi \frac{n}{a} x \right) + i \sin \left( -2\pi \frac{n}{a} x \right) \right] \\ &= \frac{1}{a} \sum_{n=0}^{\infty} F_n \exp(-2\pi i \frac{n}{a} x) = \frac{1}{a} \sum_{n=0}^{\infty} F_n \exp(-i Q_n x).\end{aligned}\tag{1}$$

Here  $n$  is an integer,  $a$  is the length of the unit cell in the  $x$  direction, and  $Q_n = 2\pi n/a$ . Figure 1b shows the first eight terms in the Fourier series for  $\rho(x)$  of  $\text{MoS}_2$ . Each term represents a stationary wave, or “Fourier component,” of scattering density whose wavelength is  $a/n$ , so that in the repeat distance  $a$  the wave undergoes exactly  $n$  oscillations. Thus the sum in Eq. 1 contains only waves that have  $a$  as a repeat distance. Each stationary wave has an amplitude  $F_n$ , which for the  $\text{MoS}_2$  structure is either positive or negative. In the most general case  $F_n$  can be complex.

Just as the displacement,  $x$ , can be represented by a vector in one-dimensional real space, the inverse wavelengths  $n/a$  ( $= Q_n/2\pi$ ) can be represented by vectors in one-dimensional “reciprocal space.” These “reciprocal-lattice” vectors define a row of equally spaced points, labeled by the values of  $n$ . All the remaining reciprocal space is empty. The points are called the “reciprocal lattice” because their spacing is  $1/a$ , the reciprocal of the real-lattice spacing. (The name “reciprocal space” has the same origin.) Their locations depend only on  $a$ , the periodicity of the real lattice, and not on the contents of the unit cell. In Fig. 1c the amplitude  $F_n$  of the  $n$ th Fourier component of  $\rho(x)$  for  $\text{MoS}_2$  is plotted at the reciprocal-lattice point  $n/a$ .

Thinking of the  $Q_n$ 's as one-dimensional vectors (the wave vectors of the Fourier components), we note from the definition of the  $Q_n$ 's and the discussion of diffraction in the primer that when the momentum transfer in a diffraction experiment  $(h/2\pi)\mathbf{Q} = (h/2\pi)\mathbf{Q}_n$ , we observe a Bragg peak whose intensity is  $S(\mathbf{Q}_n) = |F_n|^2$ . In crystallographic terminology the  $F_n$ 's are called structure factors; unfortunately the same name is used by the neutron-scattering community for  $S(\mathbf{Q}_n) = |F_n|^2$ . Whatever the nomenclature, crystallographers frequently describe crystals in reciprocal space because the quantities they measure directly are the reciprocal-lattice vectors  $\mathbf{Q}_n$  and the intensities on the reciprocal lattice  $S(\mathbf{Q}_n)/2\pi$ . Figure 2 shows a variation of Fig. 1 whose significance will be discussed later.

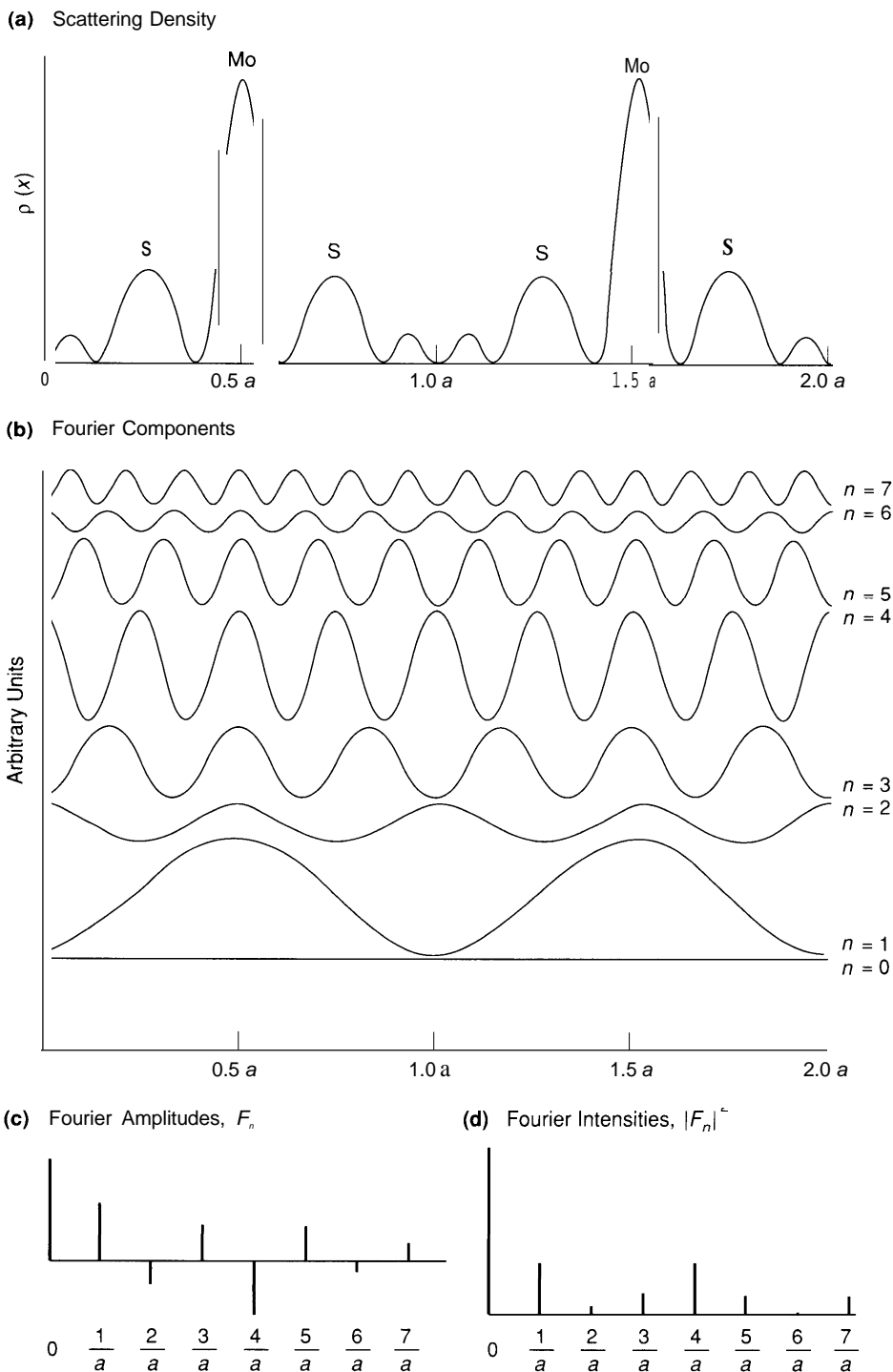
In order to extend Eq. 1 to descriptions of three-dimensional crystals, we replace  $Q_n = 2\pi n/a$  with a three-dimensional wave vector  $\mathbf{Q}_h$ . For simplicity we begin with a real lattice whose three axes are mutually perpendicular, as shown in Fig. 3a. Then the natural coordinates are orthogonal, and

$$\mathbf{Q}_h = 2\pi \left( \frac{h}{a}, \frac{k}{b}, \frac{l}{c} \right).$$

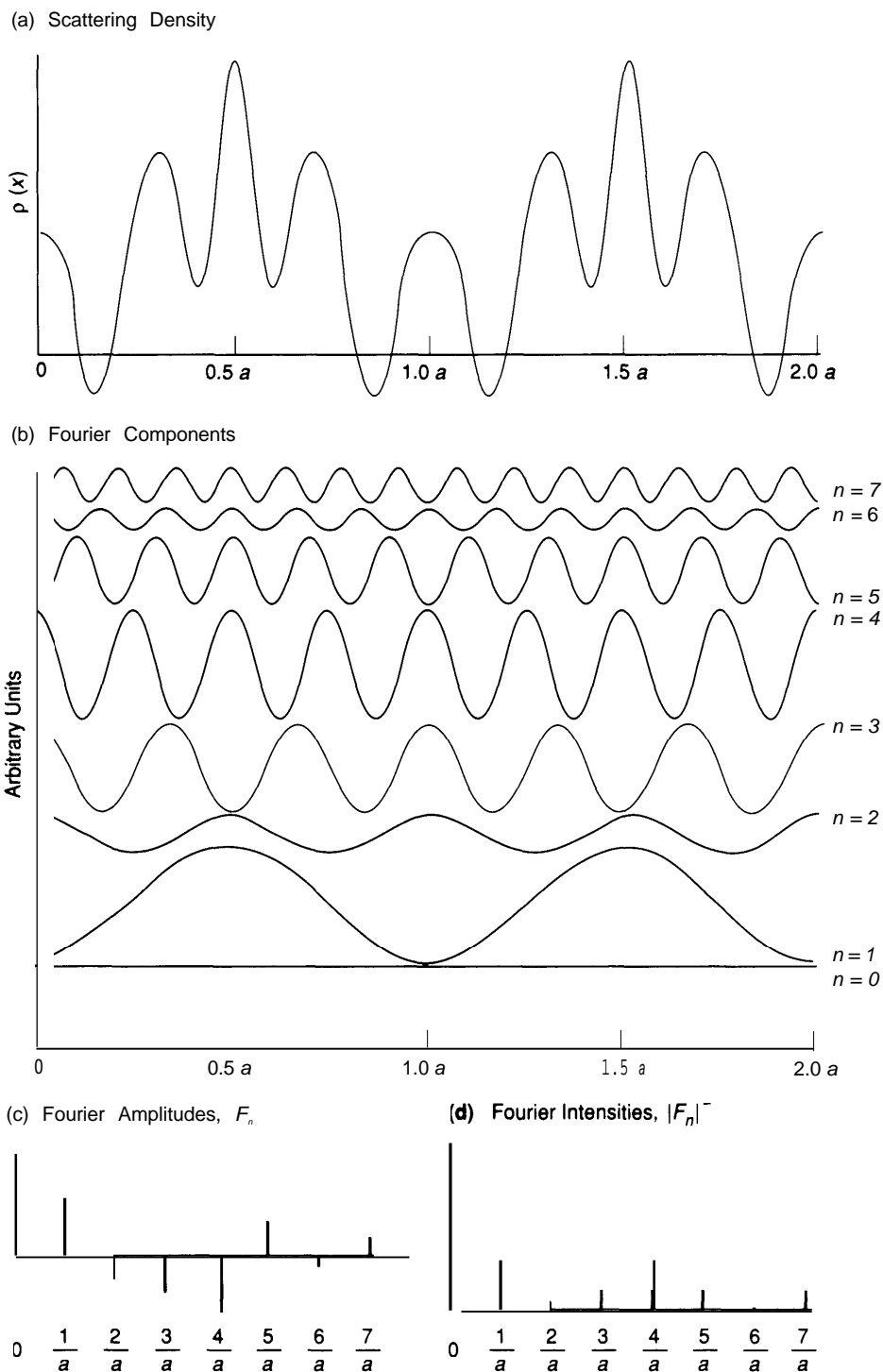
Here  $a$ ,  $b$ , and  $c$  are the repeat distances along the three axes of the unit cell, or lattice spacings, and the integer triplet  $\mathbf{h} = (hkl)$  gives the components of  $\mathbf{Q}_h$  along the three axes of the reciprocal-lattice unit cell, measured in units of the reciprocal-lattice repeat distances  $a^* = 1/a$ ,  $b^* = 1/b$ , and  $c^* = 1/c$ . Thus, in analogy with the one-dimensional case, the integer triplets  $\mathbf{h}$  specify all the possible  $\mathbf{Q}_h$  values, that is, all the wave vectors of Fourier components of the three-dimensional scattering-density distribution. Each  $\mathbf{Q}_h$  is perpendicular to a stack of parallel planes in real space, and  $2\pi/|\mathbf{Q}_h|$  (which has the dimensions of length) is the spacing between those planes, commonly called the “d-spacing”. Each  $\mathbf{h}$  labels a set of planes

**A ONE-DIMENSIONAL LATTICE AND ITS RECIPROCAL-SPACE REPRESENTATION**

**Fig. 1.** (a) The x-ray scattering density along one direction of molybdenum disulfide illustrates a one-dimensional lattice with a unit cell of length  $a$ . (b) The first eight Fourier components ( $n = 0$  to 7) in Eq. 1 for the scattering-density function in (a). The wavelength of the  $n$ th component is  $\frac{a}{n}$ . Note that the phase of some of the waves is offset by  $180^\circ$  with respect to others. (c) The amplitudes  $F_n$  of the Fourier components from (b) plotted in reciprocal space. The reciprocal lattice is the set of points  $\frac{n}{a}$  whose spacing is  $a^{-1}$ , the reciprocal of the lattice spacing in real space. Note that some amplitudes are negative (those of waves shifted in phase by  $180^\circ$  with respect to the waves with positive amplitudes). (d) The intensities  $|F_n|^2$ , or  $S(Q_n)$ , plotted in reciprocal space. This pattern of intensities would be obtained from a diffraction experiment. This pattern reveals the size of the unit cell, but as explained in Fig. 2 does not yield a unique determination of the contents of the unit cell.



perpendicular to  $Q_n$ . Together the  $\mathbf{h}$ 's specify all the sets of planes that pass through unit cells in a periodic way. Therefore just as in one dimension a sum over the wave vectors  $2\pi n/a$  with integer  $n$  sufficed to describe a periodic  $\rho(x)$ , in three dimensions a sum over the wave vectors  $Q_n$ , or over the  $\mathbf{h}$ , is all we need to describe  $p(\mathbf{r})$  for a crystal. The integer components  $hkl$  of  $\mathbf{h}$  are identical to the Miller indices that crystallographers use to label faces along which crystals break. More important, the  $Q_n$  are the special wave vectors  $Q$  at which Bragg scattering can occur, as defined in the primer. In the general case, illustrated in Fig. 3b, the  $Q_n(\equiv 2\pi(h\mathbf{a}^* + k\mathbf{b}^* + l\mathbf{c}^*))$  are still perpendicular to stacks of planes and their lengths are still equal to  $2\pi$  divided by the  $d$ -spacings. Note that the  $Q_n$  must be defined in terms of the translation vectors of the reciprocal lattice, which are no longer simply parallel to the translation



### THE PHASE PROBLEM IN CRYSTALLOGRAPHY

Fig. 2. The same as Fig. 1, except that one Fourier component has been phase-shifted by  $180^\circ$  to produce an entirely different and fictitious scattering density for  $\text{MoS}_2$ . The shifted wave and its amplitude are shown in red. This example illustrates the ambiguity that arises in diffraction experiments from measuring the magnitudes of the  $F_n$ 's but not their phases. Although the plot of the  $F_n$ 's changes, the plot of  $|F_n|^2$ , which is analogous to a diffraction pattern, does not. Thus diffraction experiments can not distinguish the scattering density in Fig. 1 from that in this figure. Determining the phases is called "solving the structure" because only then can the contents of the unit cell be determined.

vectors of the real lattice but are more complicated functions of its parameters.

Returning to the three-dimensional version of Eq. 1, we replace the product  $Q_n x$  by the dot product  $\mathbf{Q}_h \cdot \mathbf{r}$  and normalize the Fourier series by the unit-cell volume  $V_c$ :

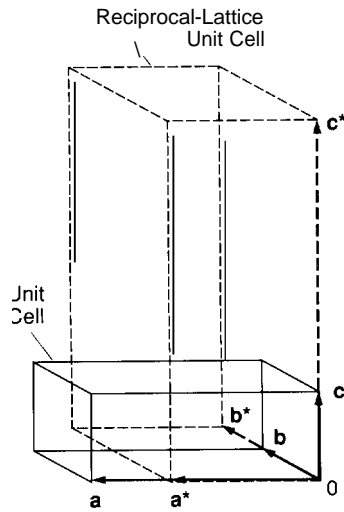
$$\rho(\mathbf{r}) = \frac{1}{V_c} \sum_{\mathbf{h}} F_{\mathbf{h}} \exp[-i(\mathbf{Q}_{\mathbf{h}} \cdot \mathbf{r})]. \quad (2)$$

(A specialist in this field would write equations such as this in crystallographic coordinates, using  $\mathbf{h}$  instead of  $\mathbf{Q}_h$  and defining  $\mathbf{r}$  in terms of displacements along the crystal axes instead of along the Cartesian directions; furthermore the displacements

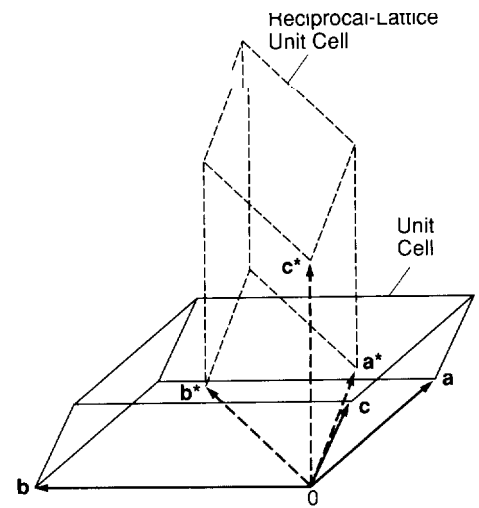
**UNIT CELLS IN REAL AND RECIPROCAL SPACE**

**Fig. 3.** (a) A unit cell in real space (solid lines) and its associated reciprocal unit cell (dashed lines), for a three-dimensional lattice whose translation vectors,  $a$ ,  $b$ , and  $c$ , are mutually orthogonal. The reciprocal-lattice translation vectors  $a^*$ ,  $b^*$ , and  $c^*$  are collinear with those of the real-space lattice, but their lengths are the reciprocals of the lengths of the real-space vectors. Note that  $a^* = Q_{100}/2\pi$  is normal to the real-space  $bc$ , or (100), plane; similarly the other reciprocal-lattice translation vectors are normal to their corresponding planes. (b) A unit cell and reciprocal unit cell for a lattice in which none of the translation vectors  $a$ ,  $b$ , and  $c$  are orthogonal. The reciprocal-lattice translation vectors  $a^*$ ,  $b^*$ , and  $c^*$  are no longer collinear with their real-space counterparts but they are still normal to the planes that bound the unit cell, and their lengths are the reciprocals of the spacings of those planes. (c) The mathematical formulae describing the reciprocal-lattice translation vectors and the wave Vectors  $Q_h$ . (d) An example of part of a set of planes and its  $d$ -spacing in a crystal whose unit cell is that shown in (b). The planes are labeled by  $h = (001)$  (parallel to the  $ab$  plane), and their  $d$ -spacing is equal to  $|c^*|^{-1}$ . In general  $Q_h \equiv 2\pi(ha^* + kb^* + lc^*)$  and  $Q_{001} = 2\pi c^*$  is perpendicular to the 001 planes.

(a) Orthorhombic Unit Cell



(b) Trigonal Unit Cell



(c) General Properties of Reciprocal-Lattice Translation Vectors and  $Q_h$

$$a^* = \frac{b \times c}{a \cdot (b \times c)}, \quad b^* = \frac{c \times a}{b \cdot (c \times a)}, \quad c^* = \frac{a \times b}{c \cdot (a \times b)}$$

$$a^* \cdot a = b^* \cdot b = c^* \cdot c = 1$$

$$Q_h = 2\pi(ha^* + kb^* + lc^*)$$

$$Q_h \perp \text{to } h \text{ planes}$$

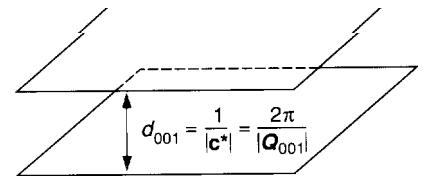
$$Q_{100} = 2\pi a^*$$

$$Q_{010} = 2\pi b^*$$

$$Q_{001} = 2\pi c^*$$

(d) Example of Set of Planes Defined by Unit Cell in (b)

(001) planes



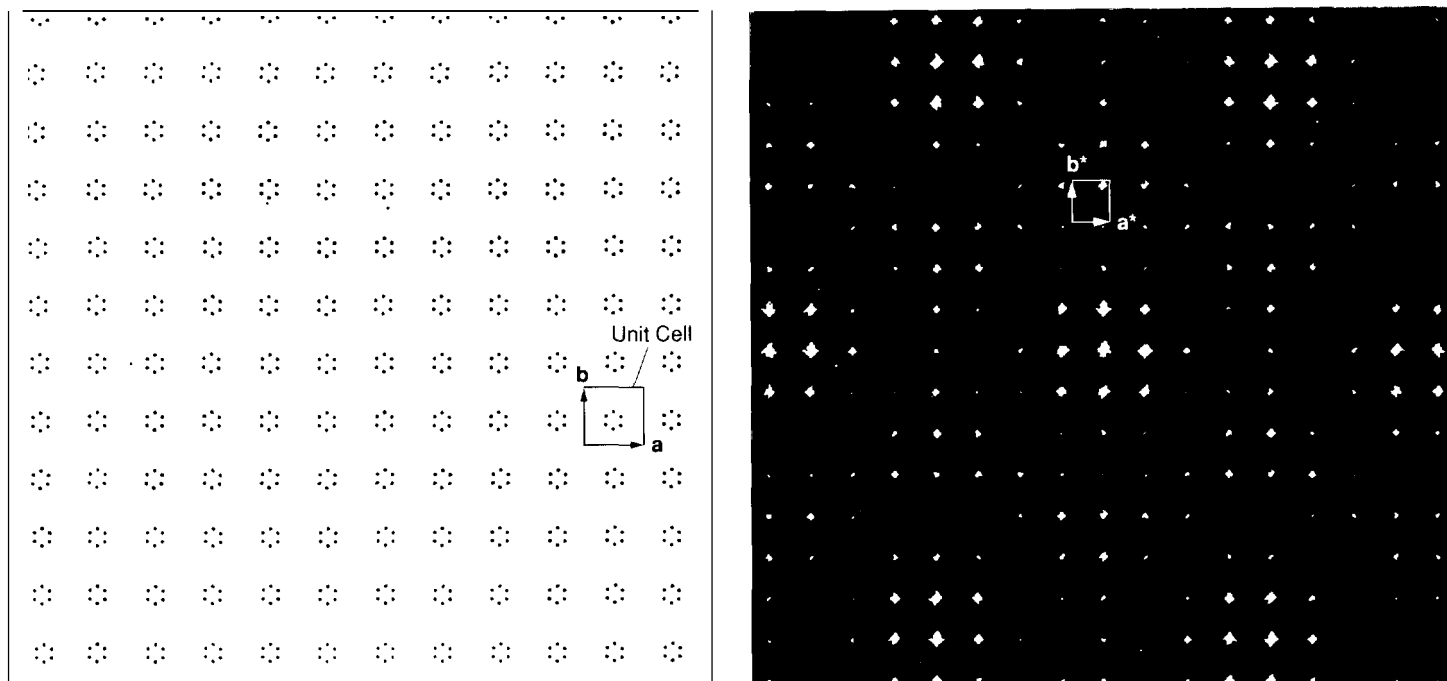
would be divided by the lattice spacings to give the components of a dimensionless vector. This shorthand is convenient for many purposes and is used in the references cited at the end of this article.) Equation 2 might appear extremely similar to the Van Hove equation for diffraction, Eq. 2 in the Primer, but it is in fact a kind of inverse. We will cover that relationship in a moment, but first we need to more fully consider what Eq. 2 implies about crystallographic mathematics.

From Eq. 2, we see that the reciprocal-space description of a crystal in three dimensions is based on an array of points defined by the vectors  $Q_h/2\pi$  and extending to infinity in all directions from a single origin. These points are the corners of an infinitely repeating reciprocal unit cell. Each amplitude  $F_h$  (positive, negative or complex) is associated with the reciprocal-lattice sites  $Q_h/2\pi$ . A complex amplitude can be represented with the usual real and imaginary parts or as a “phase shift” of the structure factor:

$$F_h = A_h + iB_h = |F_h|e^{i\alpha_h}, \tag{3}$$

where  $\alpha_h \equiv \tan^{-1}(B_h/A_h)$ . We will discuss the importance of phase shifts later in this section.

Figures 4 and 5 give examples of two-dimensional periodic scattering densities and their representations in reciprocal space (their Fourier transforms). In two dimensions the reciprocal-lattice vectors are perpendicular to sets of parallel lines (rather than planes) in real space. Larger  $h$  values correspond to more closely spaced lines.



As Figs. 4 and 5b show, the locations of the reciprocal-lattice points are determined solely by the size and shape of the real unit cell, whereas the intensities  $|F_{\mathbf{h}}|^2$  reflect the unit cell's contents. The relatively few  $F_{\mathbf{h}}$  with small  $|\mathbf{h}|$  (those closest to the origin) give only the gross features of the structure, that is, the features whose size is roughly on the order of the unit-cell dimensions. The much more numerous  $F_{\mathbf{h}}$  with large  $|\mathbf{h}|$  contain information on the fine details within the unit cell, for example, exact atom locations and anisotropic features of the thermal motion.

#### A SQUARE LATTICE AND ITS RECIPROCAL-SPACE REPRESENTATION

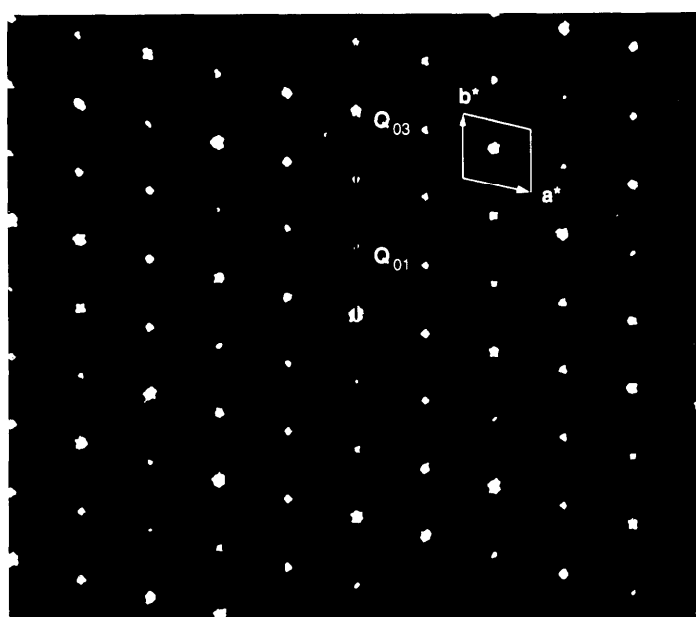
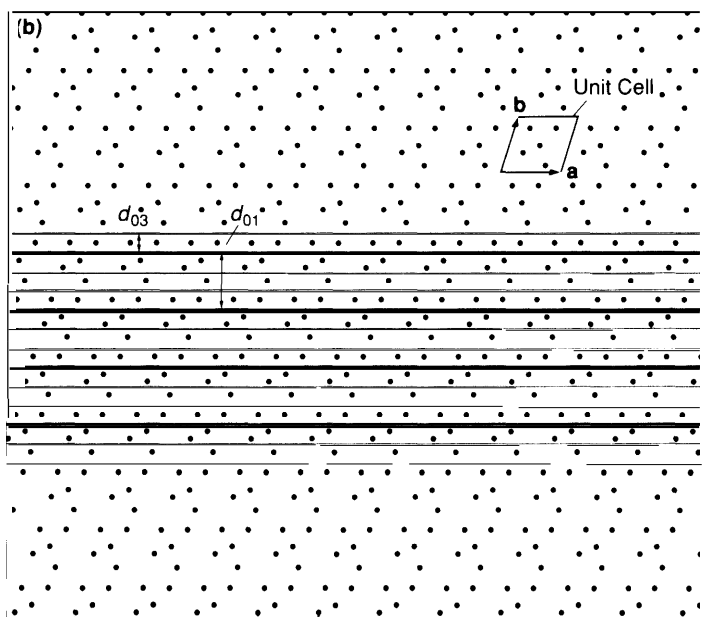
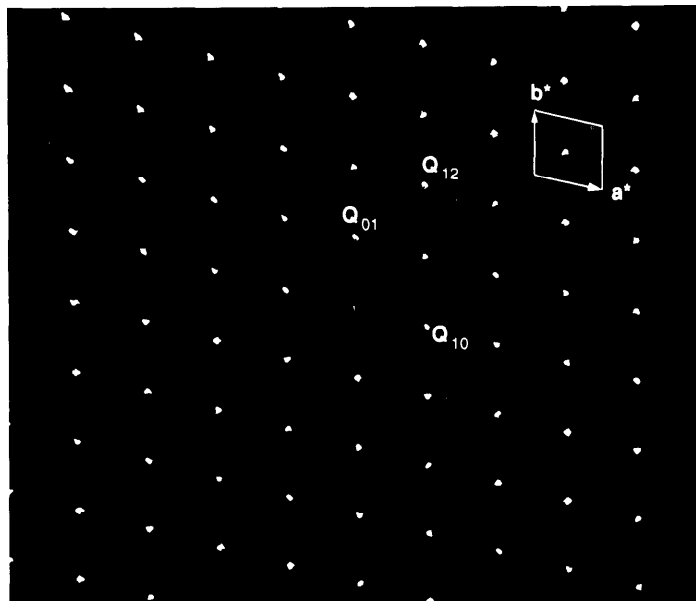
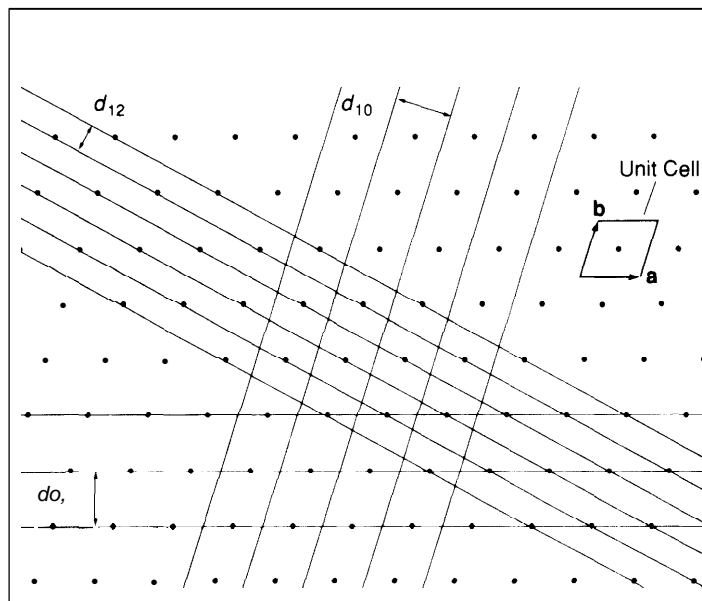
**Fig. 4.** A lattice in real space (left) with fourfold rotational symmetry and the corresponding reciprocal lattice (right), which has the same point symmetry (see “Crystal Symmetry Groups”). The intensities  $|F_{\mathbf{h}}|^2$  depicted on the reciprocal lattice differ from each other because the real-space unit cell has six point scatterers rather than one. Specifically, the pattern of intensities reflects the sixfold symmetry of the contents of the real unit cell. (Photos reproduced with permission from Cornell University Press.)

### Determining Crystal Structures

A property of Fourier series is that they can be “inverted.” In crystallography, this transformation goes from the real-space to the reciprocal-space description. Thus, the inverse Fourier transform of Eq. 2 gives the amplitude in terms of the scattering density:

$$F_{\mathbf{h}} = \int_{V_c} \rho(\mathbf{r}) e^{i(\mathbf{Q}_{\mathbf{h}} \cdot \mathbf{r})} d\mathbf{r} = \sum_{i=1}^n f_i e^{i(\mathbf{Q}_{\mathbf{h}} \cdot \mathbf{r}_i)}. \quad (4)$$

The amplitude is first expressed as an integral to indicate that all of the space within the unit cell is used. It is then expressed as a sum by using the convolution properties of Fourier integrals and series. A convolution is a type of multiplication. In this case it is used to break up the integral into a sum over all the atoms in the unit cell; the coefficient  $f_i$  of the term for the  $i$ th atom is called the “scattering factor” of that atom. The scattering factor of an atom is the Fourier transform of the scattering density in its vicinity and in this expression includes the “smearing” effect of any oscillation (or thermally induced motion) of the atom about its average position. The so-called coherent scattering length  $b_{\text{coh}, i}$  of neutron scattering is a scattering factor that does not include the effects of thermal motion. (This article deals only with coherent scattering, so in reference to scattering lengths the word “coherent” and the subscript “coh” will be suppressed from now on.) The Fourier transform represented in Eq. 2 implies that if the  $F_{\mathbf{h}}$  are known, one can calculate the scattering density  $\rho(\mathbf{r})$ , which maps the locations and thermal motions of the atoms. Similarly, the transform in Eq. 4 implies that, if the atom positions and thermal motions are known, then the  $F_{\mathbf{h}}$  can be calculated.



### SIMPLE VERSUS COMPLEX UNIT CELL IN REAL AND RECIPROCAL SPACE

Fig. 5. Two-dimensional scattering densities (left) and their corresponding intensity representation in reciprocal space (right). The real-space lattice in (a) is less symmetrical than that in Fig. 4, having two-fold rotation and inversion. The real-space figure shows a unit cell and three sets of parallel lines (the two-dimensional equivalent of parallel planes in three dimensions) with the d-spacings of those lines. Note that the set of lines indexed  $h = (10)$  is not drawn through the point scatterers, because one need not think of those lines as locations of atoms in a crystal, but rather as defining periodic density variations with a definite orientation and spacing. The other sets of lines are drawn through the point scatterers for clarity. The  $Q_h$  vectors corre-

pending to the labeled sets of lines are shown in reciprocal space (right), along with a reciprocal unit cell. Each  $Q$  vector is perpendicular to the set of lines that  $h$  indexes, and its length  $|Q_h|$  is inversely proportional to the  $d$ -spacings of that set of lines. Because the unit cell contains only a single point scatterer, the intensities  $|F_h|^2$  on the reciprocal lattice are all identical. (b) A real-space lattice in which each point in (a) has been replaced by a five-point pattern or "molecule." This scattering density does not even have inversion symmetry. The points of its reciprocal lattice are in the same positions as those of the reciprocal lattice in (a), but here the intensities  $|F_h|^2$  vary. Thus the locations of the reciprocal-lattice points provide information about lattice geometry

whereas the intensities provide information about the contents of the unit cell. The heavy lines correspond to  $h = (01)$ ; they and the light lines together have  $h = (03)$ . (The reciprocal-lattice figures were made by shining a laser beam through masks with holes punched out at the real-lattice sites and recording the diffracted light on film. With this method one can photograph much of the two-dimensional reciprocal lattice at once. Unfortunately, scattering neutrons analogously from a plane of atoms is not feasible. Neutrons interact so weakly with matter that a beam perpendicular to a single plane of atoms would pass through practically unaffected.) (Photos reproduced with permission from Cornell University Press.)

The Van Hove equation for elastic-scattering intensities given in the primer is the convolution of Eq. 4 with itself:

$$S(\mathbf{Q}_h) \equiv I_h = F_h F_h^* = \int_{V_i} \int_{V_j} \rho(\mathbf{r}_i) \rho^*(\mathbf{r}_j) e^{i\mathbf{Q}_h \cdot (\mathbf{r}_i - \mathbf{r}_j)} d\mathbf{r}_i d\mathbf{r}_j = \sum_{ij} f_i f_j^* e^{i\mathbf{Q}_h \cdot (\mathbf{r}_i - \mathbf{r}_j)}, \quad (5)$$

where  $I_h$  is the measured scattering intensity at  $\mathbf{Q} = \mathbf{Q}_h$ . Equation 5 shows how elastic-scattering experiments directly measure the  $|F_h|^2$ , the squares of the magnitudes of the structure factors. In the last form of the convolution, the double summation covers all interatomic vectors in the crystal, which matches our picture of coherent scattering as arising from interference effects between atoms. The double-integral form also reflects interference effects, since the largest contributions come from those  $\rho(\mathbf{r}_i)\rho^*(\mathbf{r}_j)$  products such that  $\mathbf{r}_i$  and  $\mathbf{r}_j$  correspond to atomic positions. In this formulation of the Van Hove equation, we recognize that both  $f_i$  and  $p(\mathbf{r})$  can be complex and that  $f_i$  has a  $\mathbf{Q}$  dependence, so we keep them inside the integral and the sum. Although  $b_i$  and  $p(\mathbf{r})$  are rarely complex in neutron diffraction, they are quite often complex in x-ray scattering because atoms can absorb x rays and because x-ray wavelengths are comparable to the size of the electron clouds from which they scatter, whereas neutrons scatter from the nearly point-like nuclei. In this discussion we have seen that by starting from a rather mathematical description of a crystal, we can interpret its coherent scattering properties for either x rays or neutrons in a particularly clean way.

The Van Hove equation gives us the relationship between the array of interatomic vectors and the observed intensities but, it also points out a major difficulty. Using Eq. 2 requires knowing both the real and imaginary parts of the  $F_h$ , but a diffraction experiment yields only the magnitudes of the  $|F_h|^2$  and not the phases  $\alpha_h$ . Without the phases we can not determine the positions of the atoms in the unit cell or even their number. The central problem of crystallography is recovery of the phases, so that the Fourier transform in Eq. 2 can be performed. The solution of this problem, known as solving the crystal structure, is the subject of considerable effort by crystallographers. The reader is encouraged to examine some of the references listed at the end of this article. Figure 2 is a one-dimensional illustration of the ambiguity. A new hypothetical scattering density  $p(x)$  has been constructed by shifting the phase of the third Fourier component in Fig. 1a by  $\pi$  radians. This shift is equivalent to multiplying that wave's amplitude,  $F_3$ , by  $-1$ , as seen in the graph of the  $F_h$  in reciprocal space, Fig. 2b. A phase shift by some angle  $\alpha$  other than 0 or  $\pi$  is equivalent to multiplying  $F_3$  by the complex number  $\exp(i\alpha)$ —hard to depict on the page. (Mathematically inclined readers can convince themselves that the  $F_h$ 's are real if and only if the unit cell is centrosymmetric, as defined in "Crystal Symmetry Groups.") In any case, the phase shift does not affect the value of  $|F_3|^2$  (Fig. 2c). Since diffraction experiments provide only the  $|F_h|^2$ , there is, in principle, no way of knowing whether the measured reciprocal lattice arises from the real-space scattering density of Fig. 1a or from the quite different density of Fig. 2a. In practice, the crystallographer realizes from his or her knowledge of physics and chemistry that the density in Fig. 2a makes no sense. Solving the structure of more complicated materials is not so easily done. Then the question is how to directly use the  $|F_h|^2$ .

One possible use is to apply a Fourier transform to the Van Hove equation to get a mapping of the interatomic vectors:

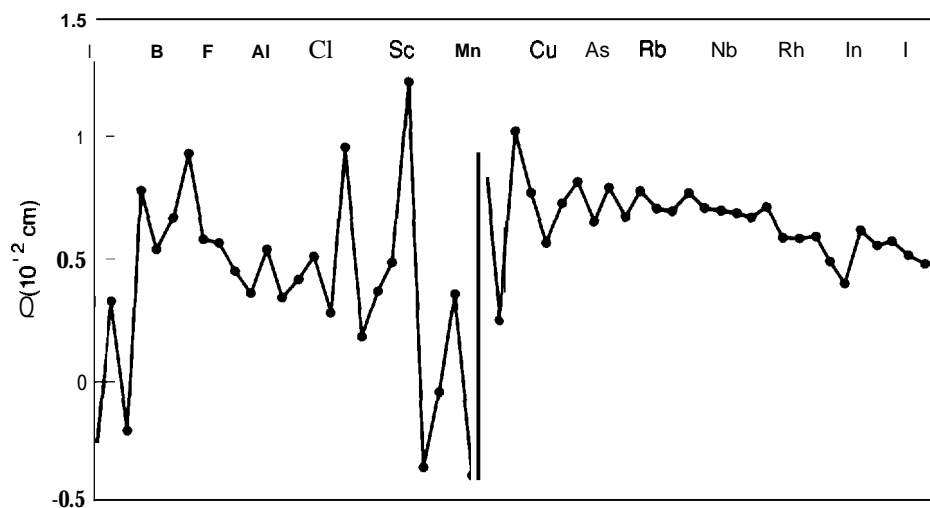
$$P(\mathbf{r}_i - \mathbf{r}_j) = \frac{1}{V_c^2} \sum_h |F_h|^2 e^{-i\mathbf{Q}_h \cdot (\mathbf{r}_i - \mathbf{r}_j)} \quad (6)$$

Equation 6 is effectively a map of the  $p(\mathbf{r}_i)p(\mathbf{r}_j)$  product for all vectors  $(\mathbf{r}_i - \mathbf{r}_j)$ . The transform can be performed with no knowledge of the crystal structure apart from the unit-cell dimensions and point symmetry, which derive directly from the

diffraction data. In crystallographic parlance  $P(\mathbf{r}_i - \mathbf{r}_j)$  is known as the Patterson function. It provides one of the routes to solving the crystal structure. Since the  $\rho(\mathbf{r}_i)\rho(\mathbf{r}_j)$  product is largest for vectors between strongly scattering atoms, the highest features in the Patterson function correspond to vectors between pairs of such atoms and can generally be interpreted to give their locations. This technique for solving crystal structures, known as the heavy-atom method, is one of the oldest techniques known. It is generally applicable only to x-ray diffraction data for materials whose unit cells are composed of one strongly scattering heavy atom (typically a metal) and

## NEUTRON SCATTERING LENGTHS

Fig. 6. Neutron scattering lengths for all the elements from hydrogen through xenon. Every fourth element is marked. Each element is made up of its natural mixture of isotopes. Unlike x-ray scattering factors, neutron scattering lengths do not increase linearly with atomic number. Instead they vary erratically, not only from element to element but from isotope to isotope.



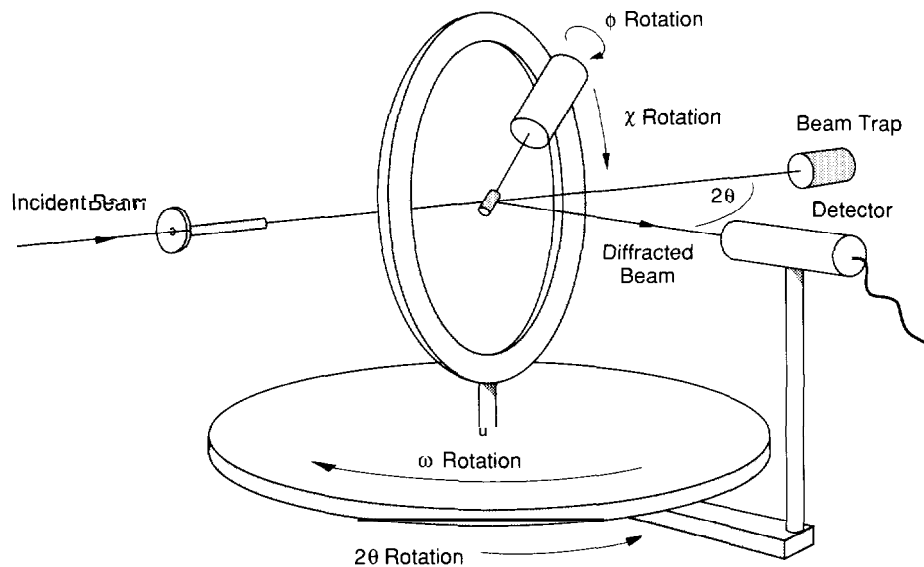
a large number of more weakly scattering light atoms (C, O, N, etc.). The heavy atom positions can then be applied to Eq. 4 to get an estimate of the phase angles to use in Eq. 2, which produces an approximation to  $p(r)$ . This scattering-density map usually shows enough atom positions to repeat the process and expand the solution to include all the remaining atom positions, thus solving the structure. The heavy-atom method is not so useful in the case of neutron scattering because the scattering lengths of all atoms are the same within an order of magnitude (Fig. 6). The other methods for solving crystal structures have their roots in the properties of the Patterson function and its inverse, the Van Hove equation. The only exception is the time-honored method of just guessing atom positions and using Eq. 4 to judge the accuracy of the guess by comparing the calculated  $|F_{\mathbf{h}}|^2$  with observations.

## The Geometry of Diffraction in Reciprocal Space

Let's consider diffraction experiments that use monochromatic beams, that is, those such that all the neutrons or x rays have the same wavelength  $\lambda$ . Then, as noted in [the discussion following Eq. 3 of the primer, one can see Bragg peaks only when the planes that produce them are properly oriented with respect to the beam. In a single-crystal diffraction experiment, the crystal is rotated, in an apparatus like that shown in Fig. 7, so as to generate Bragg reflections with various values of  $\mathbf{h}$ . Then the detector is positioned to measure their  $|F_{\mathbf{h}}|^2$ . A powder experiment involves many crystals at once, all randomly oriented. We need to understand the effect of different crystal orientations in both single-crystal and powder experiments.

As we have seen, the  $\mathbf{Q}_{\mathbf{h}}$  vectors are perpendicular to sets of planes of the crystal, and the  $\mathbf{h}$  vectors correspond to the Miller indices that describe its faces. Thus there is a connection between the physical appearance of a crystal and its reciprocal-space description. Real space and reciprocal space are "hooked" together (see Fig. 3) so that every feature found in real space corresponds to a feature in reciprocal space via Fourier transformation. Therefore when we rotate the crystal, we also rotate its reciprocal lattice.

Figure 8 depicts Bragg scattering in reciprocal space. In terms of the reciprocal-lattice vectors, we can write Bragg's law simply as  $|\mathbf{Q}| = |\mathbf{Q}_h|$ , using  $|\mathbf{Q}| = 4\pi(\sin\theta)/\lambda$  (see Fig. 5a of the Primer) and  $|\mathbf{Q}_h| = 2\pi/d_h$  where  $d_h$  is the spacing of the planes labeled by  $\mathbf{h}$ . Thus depicting the elastic-scattering triangle (again in Fig. 5a of the primer) in reciprocal space provides a useful geometric construction (here we multiply all the reciprocal-lattice distances by  $2\pi$  in order to compare them with wave vectors). Since for elastic scattering the initial and final wave vectors are equal in magnitude, or  $|\mathbf{k}_i| = |\mathbf{k}_f|$ , all the possible  $\mathbf{k}_f$ 's fall on the surface of a sphere with ra-



## SINGLE-CRYSTAL DIFFRACTOMETER

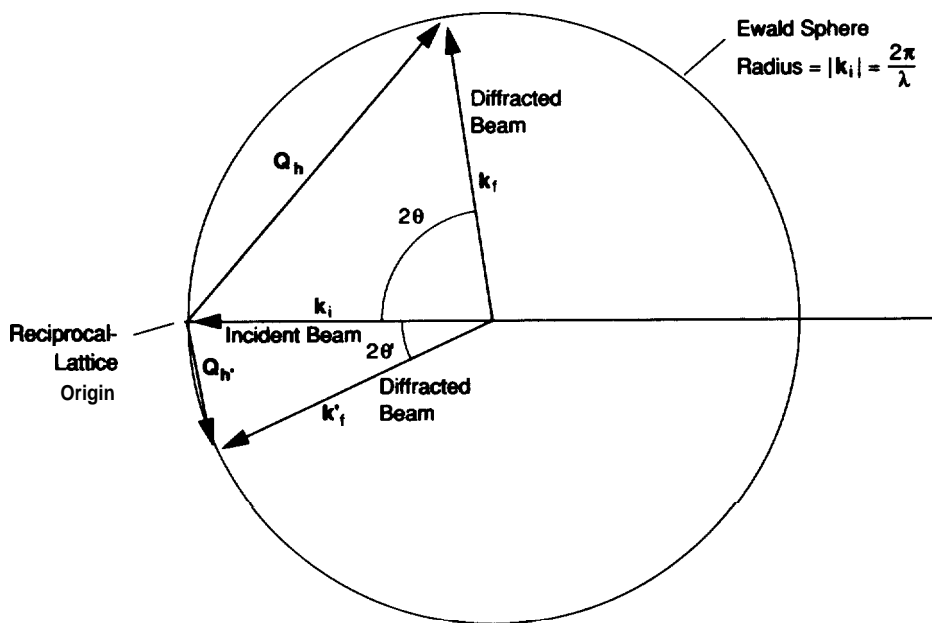
Fig. 7. A single-crystal diffractometer with three axes for positioning the crystal in the incident beam so that a particular set of planes in the crystal scatters the incident radiation in the plane containing the detector arm. The detector angle can be set at the proper  $2\theta$  to observe the reflection (once a preliminary x-ray experiment has determined the orientation and size of the reciprocal unit cell).

dius  $2\pi/\lambda$ , commonly called the Ewald sphere. As seen in Fig. 8, the Ewald sphere passes through the origin because  $\mathbf{Q} = \mathbf{O}$ , or equivalently  $\mathbf{k}_i = \mathbf{k}_f$ , corresponds to elastic scattering in the forward direction. The  $\mathbf{Q}_h$  of a reciprocal-lattice point that falls on the Ewald sphere is equal to the  $\mathbf{Q}$  at which Bragg scattering occurs; the scattering angle  $2\theta$  between  $\mathbf{k}_i$  and  $\mathbf{k}_f$  is shown on the figure. The construction makes it easy to see the effect of rotating the crystal. When the crystal rotates, the reciprocal lattice rotates with it so that each of its points moves on an arc centered at the origin. As each point passes through the Ewald sphere, diffraction occurs for that  $\mathbf{Q}_h$  at the corresponding scattering angle  $\theta$ . This is the basis for conventional single-crystal diffraction experiments. The intensity of the scattering seen by the detector when  $\mathbf{Q}_h$  passes through the Ewald sphere is proportional to  $|F_h|^2$ , but it also depends on the angle that the  $\mathbf{Q}_h$  arc makes with the sphere surface (the so-called Lorentz correction to the intensities).

Because a powder consists of a multitude of small crystals, the reciprocal-space picture has to be modified from that given for a single crystal. Instead of an array of points, the  $\mathbf{Q}_h$  vectors define a set of nested spheres, each one corresponding to the multitude of directions that each  $\mathbf{Q}_h$  points for all the crystals that make up the powder (Fig. 9). Then the orientation of the powder sample is immaterial, and the Ewald sphere for the illuminating radiation intersects all the  $\mathbf{Q}_h$  spheres with  $|\mathbf{Q}_h| < 4\pi/\lambda$ . Thus diffraction occurs simultaneously at a variety of angles. The observed intensity again depends on  $|F_h|^2$ , and the Lorentz correction depends on the angle at which the Ewald sphere and the  $\mathbf{Q}_h$  sphere intersect. In addition, the crystal symmetry may require that related  $\mathbf{h}$  vectors have the same length and therefore that their respective spheres exactly coincide. For example, in the cubic crystal structure for salt (NaCl), the  $\mathbf{Q}_h$  vectors with  $\mathbf{h} = (1\ 0\ 0)$ ,  $(0\ 10)$ ,  $(00\ 1)$ ,  $(1\ 0\ 0)$ ,  $(0\ -1\ 0)$ , and  $(00\ -1)$  all have identical lengths and identical  $F_h^2$  values. The measured intensity at the corresponding angle is proportional to  $6|F_{100}|^2$ ; the factor of 6 is the reflection multiplicity. A powder pattern then contains all the intensity information inherent in the reciprocal

## SINGLE-CRYSTAL DIFFRACTION IN RECIPROCAL SPACE

Fig. 8. A reciprocal-space representation of single-crystal diffraction of monochromatic radiation of wavelength  $\lambda$ . A sphere of radius  $|\mathbf{k}_i| = 2\pi/\lambda$  is drawn through the origin of the reciprocal lattice—the “Ewald sphere.” Since diffraction is an elastic process, the wave vectors of the incident and scattered radiation,  $\mathbf{k}_i$  and  $\mathbf{k}_f$ , have equal length and can be drawn so that they are radii of the sphere. A few of the points of the reciprocal lattice touch the surface of the Ewald sphere. Note that the  $\mathbf{Q}_h$  vector for each such point coincides with  $\mathbf{Q}$ , the third side of the scattering triangle. In other words,  $\mathbf{Q} = \mathbf{Q}_h$  (a version of Bragg’s law) and diffraction occurs at the angle  $2\theta$  between  $\mathbf{k}_i$  and  $\mathbf{k}_f$ . Rotation of the crystal corresponds to rotating the reciprocal lattice, causing other points to touch the Ewald sphere and diffraction to occur at other scattering angles.



lattice, but all the directions of the vectors are lost along with the phases of the structure factors. This situation was neatly summarized long ago by W. H. Bragg in his 1921 Presidential Address to the Physical Society.

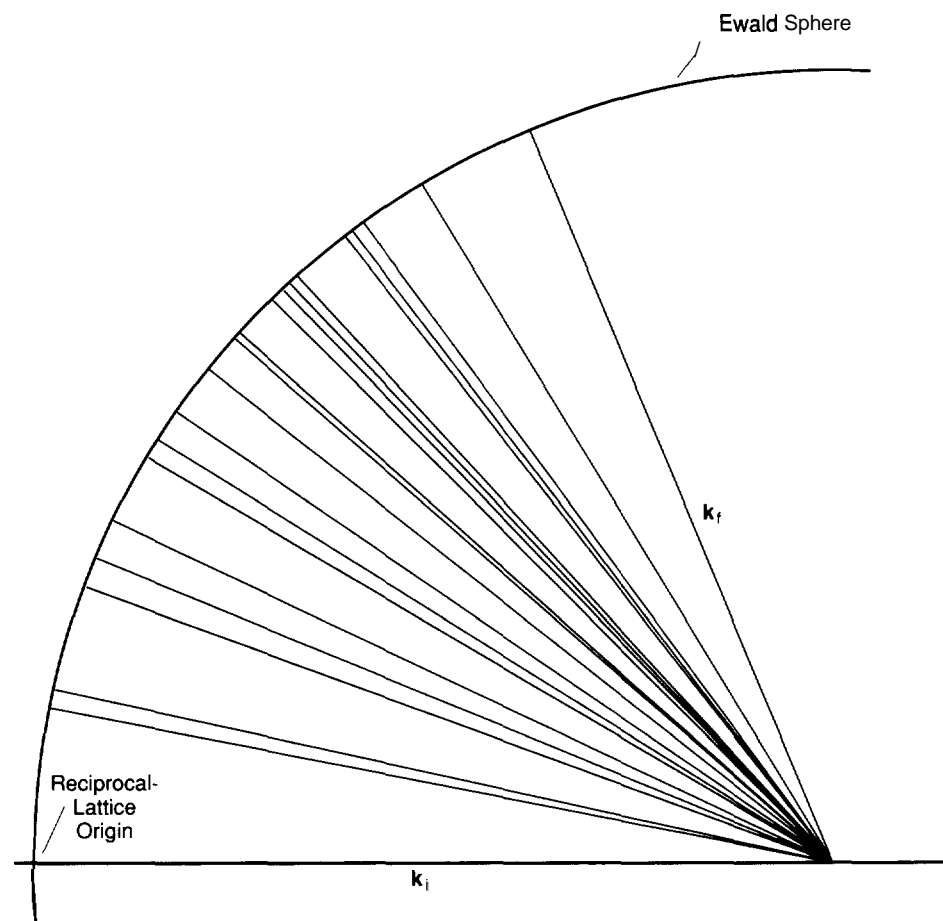
*All the spectra of the different planes are thrown together on the same diagram, and must be disentangled. This is not so difficult as it might seem. ... The spectra of the organic substances show how very diversified they are, and illustrate the power of a method of analysis which promises to be of great use, since every crystal has its own characteristic spectrum.*

Despite Bragg’s optimism about interpretation of a powder pattern, only recently has there been any real progress in powder pattern analysis. The classical use of x-ray powder patterns has been analytical, to enable identification of crystalline phases in an unknown mixture. This is usually achieved by matching the line positions and relative intensities against a compendium of such values obtained by measuring patterns of pure materials. Commercial x-ray powder diffractometers come with software packages that do the matching automatically. The computer file of standard materials maintained by the Joint Commission on Powder Diffraction Standards now contains over 50,000 entries. Our problem, however, is to unravel a powder pattern and extract the crystal structure responsible for the observed intensity distribution.

## Crystal Structures from Powder Patterns

For a long time the only way a powder pattern could be interpreted to give the crystal structure was a variation on the methods used for single-crystal diffraction data. The first step consists of identifying the vectors  $\mathbf{h}$  (or  $h, k, l$ ), that give rise to the peaks in the pattern thus identifying the crystal lattice and its parameters  $a, b$ , and  $c$ . This process, known as indexing the pattern, can be complex for low-

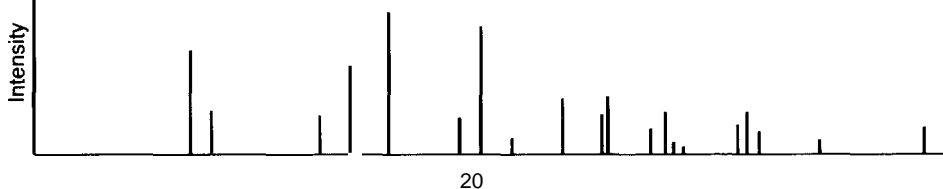
## (a) Reciprocal-Space Geometry



## POWDER DIFFRACTION IN RECIPROCAL SPACE

Fig. 9. (a) A reciprocal-space representation of powder diffraction of monochromatic radiation. The reciprocal-lattice points for a powder are smeared out onto the surfaces of a nested set of spheres, all of which intersect the Ewald sphere if  $dh \geq A/2$ . Thus diffraction from all planes whose  $d$ -spacing is greater than or equal to  $A/2$  can be recorded in a single measurement with single-wavelength radiation. (b) The powder diffraction pattern that would be recorded from a crystal having this reciprocal lattice. For clarity, the intensities are shown here but are not plotted on the reciprocal lattice in (a) (whereas they were in Figs. 4 and 5).

## (b) Powder-Diffraction Pattern



symmetry crystals but is quite easy for cubic structures. In that case the relationship between  $\mathbf{h}$  and  $d$ -spacing gives

$$d^2 = \frac{a^2}{h^2 + k^2 + l^2} \quad (7),$$

where  $a$  is the cubic-lattice spacing. One need only number the peaks starting from the origin, skipping those numbers that are not sums of three squares of integers (7, 15, 23, 28, etc.), and then tally up the possible  $hkl$  combinations for each peak. Then the intensities of individual peaks are measured and converted to structure factor magnitudes. These could then be used to “solve” the structure (remember this is a puzzle because of the lost complex character of  $F_{\mathbf{h}}$ ). The main problem with this technique is that only for very simple structures are the peaks in a powder pattern sufficiently separated to allow measurement of individual peak intensities. One can index the pattern of almost any substance and thus find a description of the lattice. However, the peaks are usually so heavily overlapped that extraction of individual peak intensities is impossible, and the magnitudes of most of the individual structure factors are unknown.

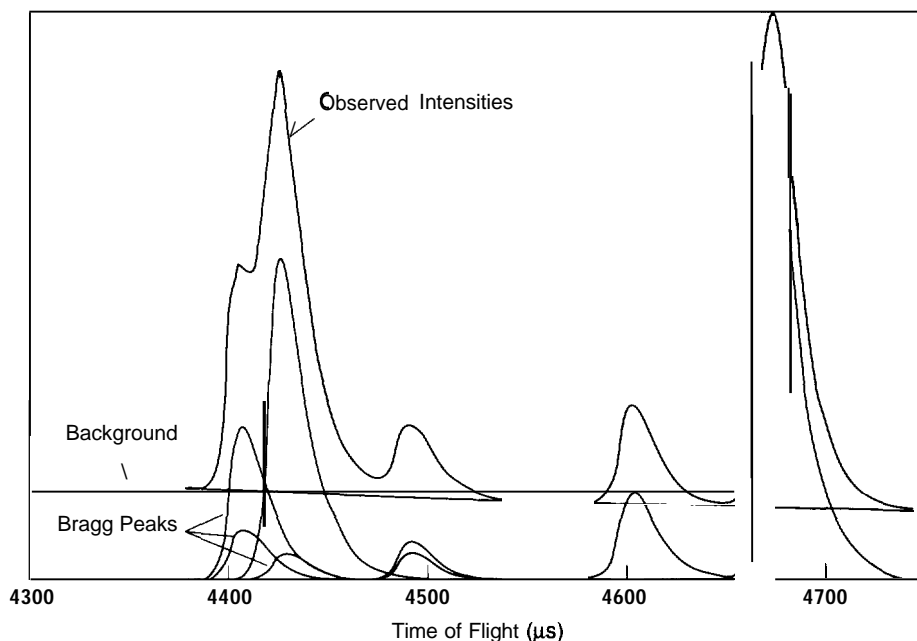
About twenty years ago H. M. Rietveld suggested a solution to this problem. He recognized that a mathematical expression could be written to represent the observed intensity  $I_c$  at every position  $Q$  in a powder-diffraction pattern:

$$I_c(\mathbf{Q}) = I_b(\mathbf{Q}) + \sum I_h(\mathbf{Q}). \quad (8)$$

This expression has a contribution from the background and from each of the  $\mathbf{Q}_h$  that are in the vicinity of  $Q$  (Fig. 10). Unlike the stick-diagram representation of a pow-

### OVERLAPPING PEAKS IN A POWDER DIFFRACTION PATTERN

Fig. 10. A small segment of a *time-of-flight* powder-diffraction pattern showing the total intensity and contributions to it from background and from several Bragg reflections. Note that four Bragg reflections contribute to the left-most observed peak.



der pattern shown in Fig. 9, a real powder pattern suffers from line broadening, so diffraction from the planes labeled by  $\mathbf{h}$  contributes not only at  $Q_h$  but at all nearby  $Q$ . The pattern in Fig. 10 also exhibits line anisotropy, which arises from the asymmetry of the spallation-neutron pulse. In the Rietveld method one models the observed pattern by considering the factors that affect both the line shape and its intensity. The adjustable parameters for the model are then refined by a nonlinear least-squares process that is similar to the process very commonly used in single-crystal x-ray structure analysis. The  $|F_h|^2$  parameters obtained from the fit are a reconstruction of the real  $|F_h|^2$ ; the parameters for line broadening and anisotropy provide information about particle sizes, structural defects, and other phenomena that distort the ideal Bragg pattern.

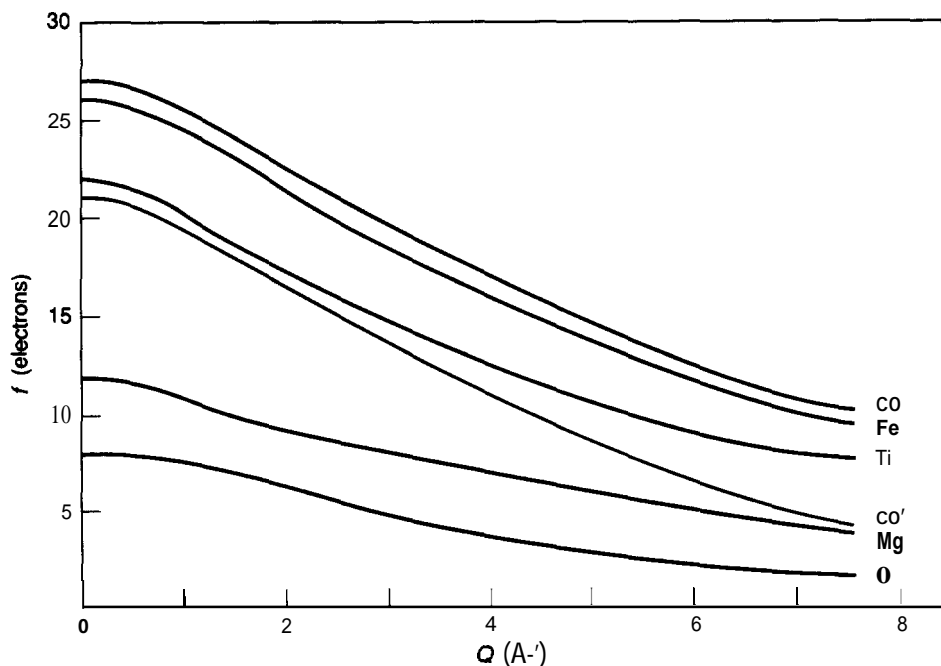
This approach has been so successful that it has led to a renaissance in powder diffraction, and this technique of treating powder-diffraction data is now known as Rietveld refinement.

### How Are X-Ray and Neutron Diffraction Complementary?

In generating a model to perform the inverse Fourier transform shown in Eq. 4, we postulate a set of atom positions and assign a scattering factor  $f_i$  to each atom, which is the Fourier transform of the scattering density about its position. However, because x rays and neutrons scatter by different mechanisms, the corresponding scattering factors are quite different. Neutrons are scattered primarily by atomic nuclei. Since the nuclear dimensions are roughly 100,000 times smaller than the neutron wavelength, the nuclei act like point scatterers and neutron scattering factors (scattering lengths or  $b$ 's) are independent of  $1/Q$ . Also, nuclear scattering is a combination of "potential" scattering and "resonance" scattering. Potential scattering depends on

the number of nuclear particles and resonance scattering results from neutron absorption by the nucleus. These two factors sometimes add and sometimes subtract to give neutron scattering lengths that vary erratically from one element to another and from one isotope to another (see Fig. 6).

On the other hand, x-ray scattering occurs primarily by interaction with the electrons that surround an atom. Consequently, the strength of the scattering depends on the number of electrons that surround an atom so that the scattering power of an atom increases with atomic number. Thus, x-ray scattering factors are usually ex-



## X-RAY SCATTERING FACTORS

Fig. 11. X-ray scattering factors for the atoms O, Mg, Ti, Fe, and Co. The gray curve labeled Co' gives the scattering factor of Co when the energy of the incident x rays is a few eV below the  $K$  absorption edge of Co. At this energy, anomalous dispersion reduces the scattering factor by about 6 electrons at all  $Q$ .

pressed as some multiple of the scattering power of one electron. In addition, the spatial extent of the electron cloud around an atom is roughly the same as the x-ray wavelength, so the x-ray scattering factor falls off with increasing  $|\mathbf{Q}|$ . The scattered intensity also has a contribution from anomalous dispersion when the x-ray energy is near an absorption edge for the scattering atom. The absorption edge for an inner electron shell of an element is the minimum energy at which an atom can absorb an x ray and consequently eject an electron from that shell. The scattering factor can be strongly modified by this process and acquire both real and imaginary components that are only partially dependent on  $|\mathbf{Q}|$ . Thus the scattering factors for x rays look like those shown in Fig. 11.

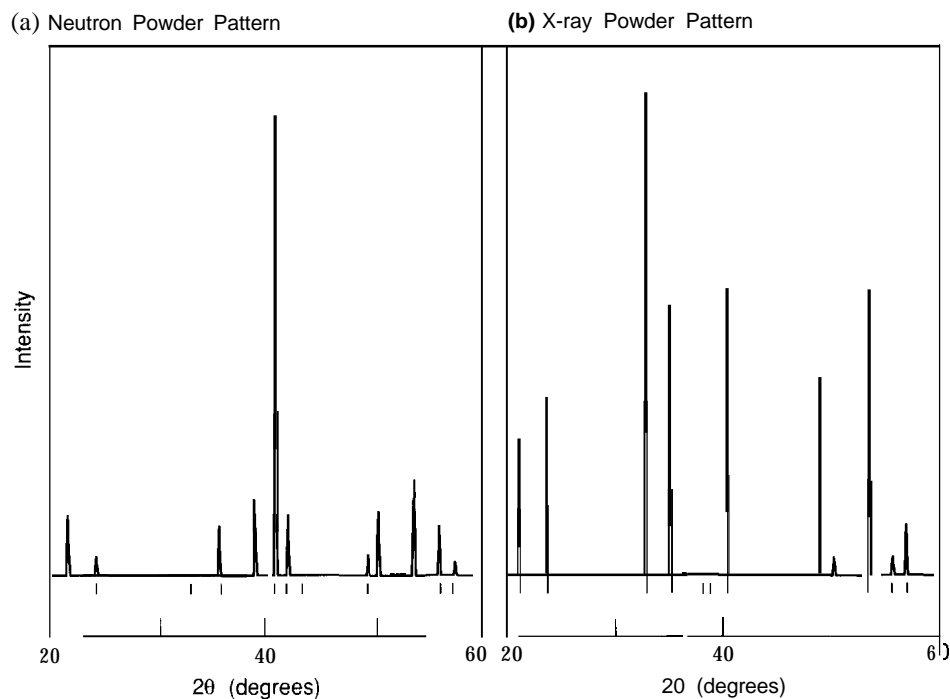
Given these differences we would expect x-ray and neutron powder-diffraction patterns to be very different. Figure 12 shows idealized x-ray and neutron patterns calculated for  $\text{MgTiO}_3$ , the primary constituent of the mineral *geikielite*. The patterns were generated for essentially identical diffractometer experiments (impossible in real life) but are startlingly different. In fact, the strongest peak in the x-ray pattern (at about  $32^\circ$ ) is completely absent in the neutron pattern! The reason for the extreme difference between the two patterns lies in the scattering factors for titanium, magnesium, and oxygen for x-rays and neutrons. The x-ray scattering factors are simply proportional to the atomic number; thus  $f_{\text{Ti}} > f_{\text{Mg}} > f_{\text{O}}$ . However, the neutron scattering length of titanium is negative and that of oxygen is only slightly larger than that of magnesium, or  $b_{\text{O}} > b_{\text{Mg}} > 0 > b_{\text{Ti}}$ . Therefore the neutron structure factor for each reflection is very different from the x-ray structure factor, and the peak heights in the two powder-diffraction patterns are very different.

The complementarity of x-ray and neutron powder patterns then eliminates one of the most basic problems in crystal-structure analysis. Because the complex nature of the structure factors is lost in any diffraction measurement and the directional

character of reciprocal space also is lost in a powder-diffraction experiment, the Rietveld refinement of a single powder pattern may not yield a unique answer. Clearly, if a crystal-structure model of atom positions, etc., produces calculated patterns that match both a neutron powder pattern and an x-ray powder pattern, that model is more likely to be unique (and correct). To capitalize on this notion we have developed a computer program that will perform a combined x-ray and neutron Rietveld refinement of a crystal structure. The remainder of the article presents some applications of this approach.

### DIFFERENCES BETWEEN X-RAY AND NEUTRON POWDER PATTERNS

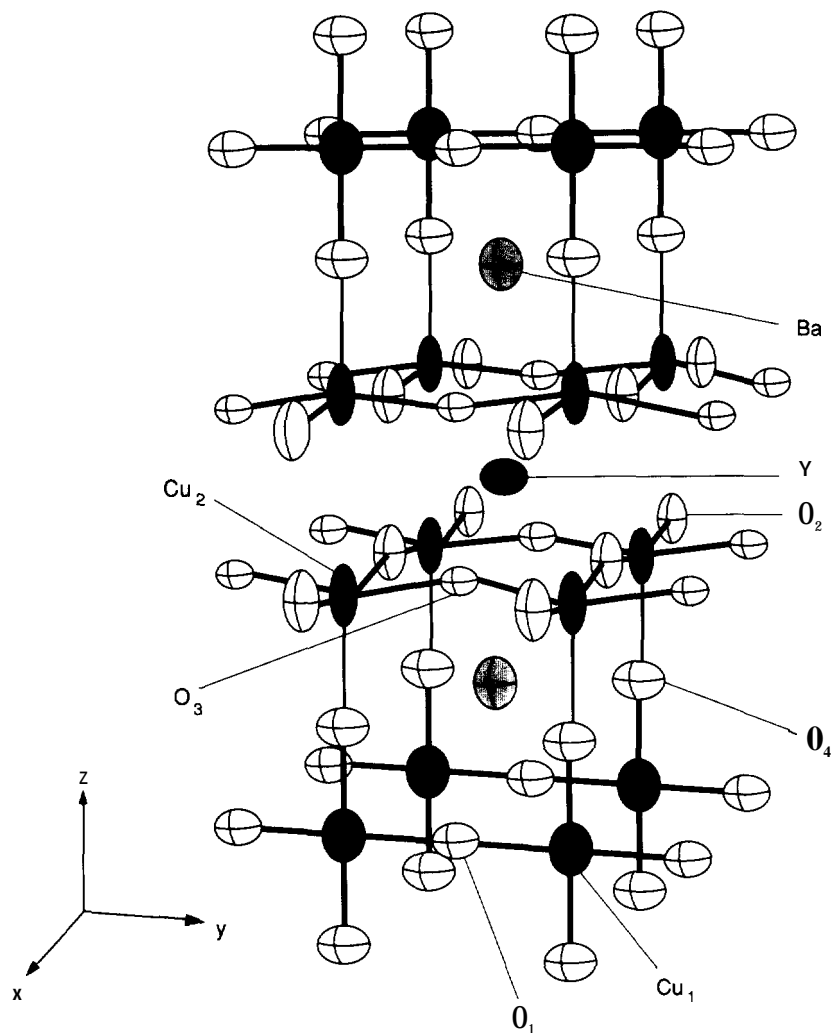
**Fig. 12.** A comparison of simulated x-ray and neutron powder patterns for MgTiO, at a wavelength of 1.54 Å. The neutron scattering lengths of Mg, Ti, and O are very different from their x-ray scattering factors, so peaks that are prominent in one pattern are small or even invisible in the other. Thus the two patterns give different information about the structure of the crystal.



### Examples of Combined Rietveld Refinements

One of the most difficult structural problems is to determine the identity of the atoms that occupy a particular site within a crystal structure. Generally an atom is identified by its scattering power relative to the other atoms in the structure. In addition, the distances between it and its nearest neighbors also help in this identification process. The large body of structural work in the literature provides the expected interatomic distances for a particular pair of atoms. The problem becomes much more difficult, however, when more than one kind of atom can occupy a particular site.

**The 123 High-Temperature Superconductor.** Our first example of an atom-identification problem concerns the high- $T_c$  123 superconductor  $\text{YBa}_2\text{Cu}_3\text{O}_{7-x}$ . This material had been investigated at great length by many groups throughout the world, and its structure had been established with little ambiguity within a few months of its discovery by Chu and coworkers at the University of Houston. Almost all structural results came from Rietveld refinements of neutron powder-diffraction data obtained at either reactor or spallation sources, and the atom identities were assigned largely by analogy to other structures as well as by their scattering powers. By unfortunate coincidence the neutron scattering lengths of yttrium and copper are virtually identical, leaving open the possibilities that the assignments of these two atom locations were in fact reversed or that each site was sometimes occupied by yttrium and sometimes by copper. Either case would have considerable impact on any theory proposed to explain the superconductivity. However, the x-ray scattering factors for these two atoms are very different, and by combining some x-ray powder data with the neutron data one can easily resolve this ambiguity.



### A HIGH- $T_c$ SUPERCONDUCTOR

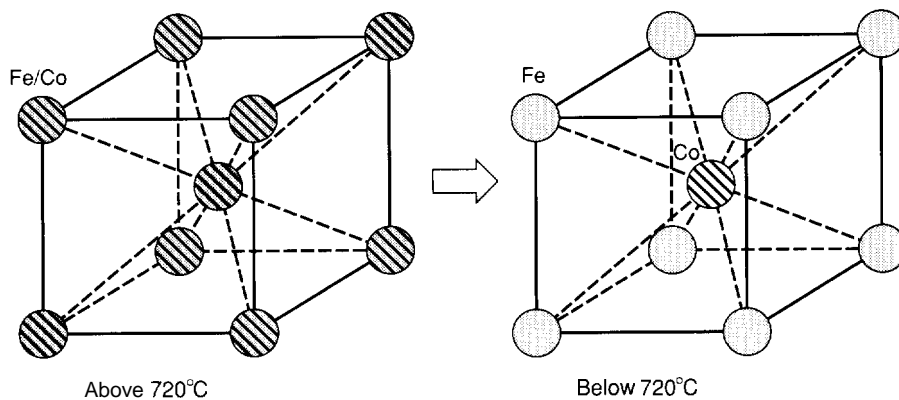
Fig. 13. A perspective drawing of the structure of  $\text{YBa}_2\text{Cu}_3\text{O}_{7-x}$  as deduced from a combined x-ray and neutron Rietveld refinement. The ellipsoids represent the extent of 99% of the atomic thermal motion. The Cu and O stems are labeled with numbers to distinguish inequivalent locations. Combined x-ray and neutron data proved that there is no interchange between the Cu atoms at these sites and the Y atoms at the site in the middle of the figure.

Here at LANSCE we performed both time-of-flight neutron and x-ray powder-diffraction experiments, collecting six powder patterns for this material. The entire set, comprising about 25,000 data points, was subjected to a combined Rietveld refinement involving approximately 120 adjustable parameters. These parameters included the 33 needed to describe the crystal structure of  $\text{YBa}_2\text{Cu}_3\text{O}_{7-x}$ , namely, atomic positions, fractional occupancies, thermal parameters, and lattice parameters. The rest characterized details of the powder-diffraction patterns and included coefficients for the background, the peak shapes, and intensity correction factors as well as the six scaling factors. The resulting structure, shown in Fig. 13, was dramatically more precise than any of the previous single-measurement results and satisfactorily resolved the metal-site occupancy issue. We found no evidence of any interchange between the metal atoms on their respective sites. Our result had been expected from crystal-chemistry considerations based on comparison of interatomic distances and ionic radii, but this work provided a clear and unambiguous determination.

**Vanadium-Doped Iron-Cobalt Alloy.** The atom-identification problem in our second example is considerably more difficult. The alloy FeCo is well known as an excellent soft ferromagnet with a high saturation magnetization and low permeability and is of great use commercially. To improve its machinability, a small amount of vanadium (about 290) is added to the alloy. This alloy is also a well-known example of a second-order  $\beta$ -brass transition: At high temperatures the two metals occupy sites of the body-centered cubic structure at random, but below 720° C the alloy orders so that atoms of the two metals tend to occupy alternate sites (Fig. 14). It had been presumed that in the low-temperature phase the vanadium atoms randomly oc-

### ORDER-DISORDER TRANSITION IN THE ALLOY FeCo

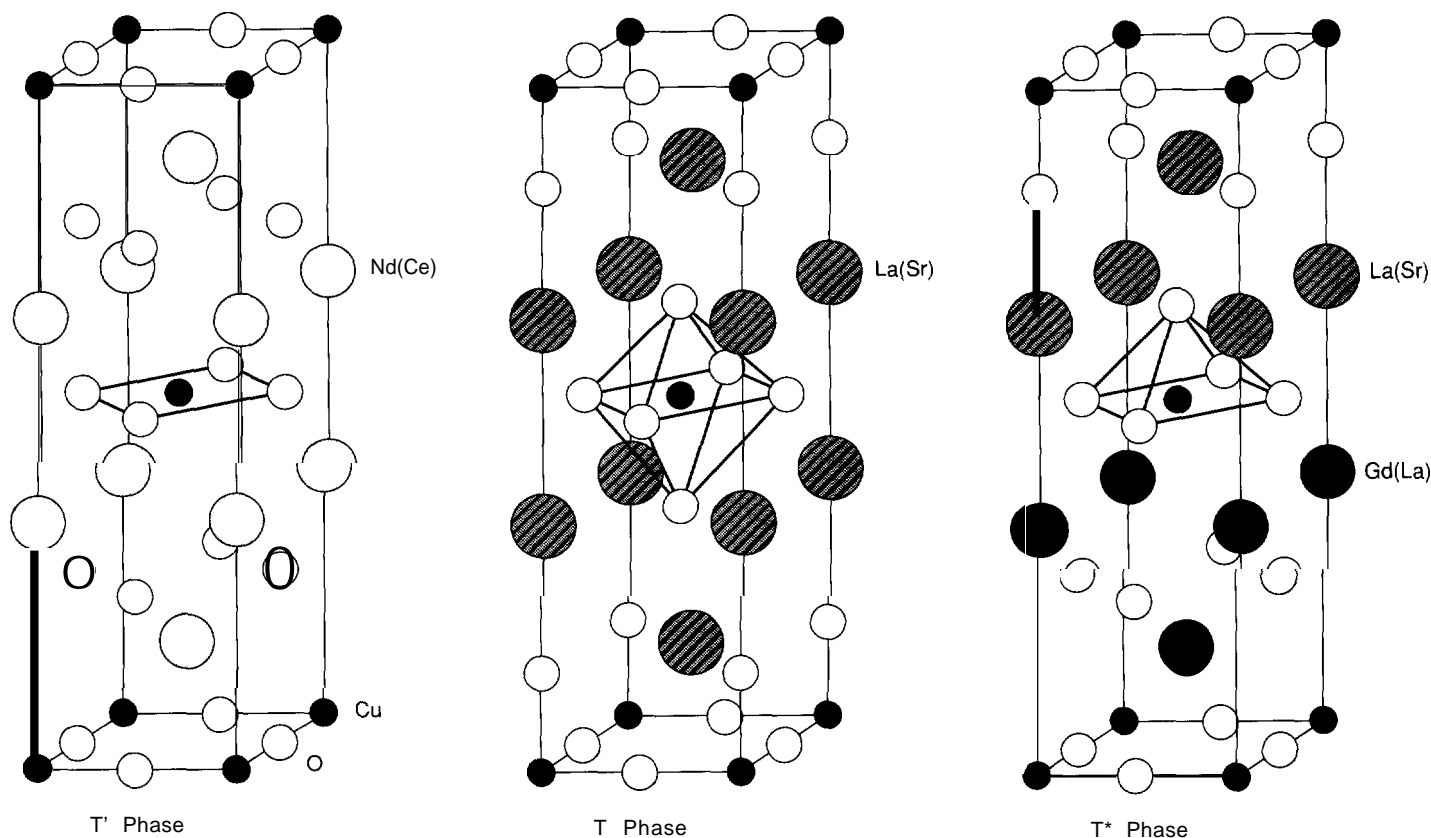
Fig. 14. A schematic representation of the  $\beta$ -brass transition in FeCo, the iron-cobalt alloy containing equal quantities of Fe and Co. In the high-temperature form on the left, each site is occupied at random by either Fe or Co. The alloy becomes ordered below 720° C to form the structure on the right. Each Fe stem is surrounded by Co stems, just as the Co stem in the figure is surrounded by Fe stems.



distribution problem by collecting neutron time-of-flight and shortwavelength x-ray data sets that covered a range of  $Q$  sufficient to independently determine the thermal-motion parameters. In addition, we performed synchrotron x-ray experiments at Stanford University. The tunability of synchrotron x-ray radiation allowed us to strongly modify the x-ray scattering factors of the three metals by collecting powder data near each of their respective  $K$  absorption edges. The strong anomalous dispersion reduced the x-ray scattering factor for each metal in turn by about 6 to 8 electrons from the dispersionless value given in Fig. 11 and thus provided sufficient contrast between that atom and the others. The entire suite of data, consisting of some 18 powder patterns with a total of about 22,000 data points, was subjected to a combined Rietveld refinement to determine the fractional occupancies for Fe, Co, and V at the two sites. The result clearly showed that the V strongly preferred the Co-rich site over the Fe-rich site and that for this particular sample the Fe/Co ordering was  $\sim 80\%$ . These results are not obtainable by any other means.

**T\*-Phase High-Temperature Superconductors.** Our final example is an extension of the idea used for the FeCo alloy. The problem is to determine the site preferences of the strontium, lanthanum, and rare-earth ions in the so-called  $T^*$ -phase superconductors. These materials have the general formula  $\text{La}_{1.8-x}\text{R}_x\text{Sr}_{0.2}\text{CuO}_4$ , where R is a rare-earth metal, and all have approximately the same structure. They have been synthesized with all the rare earths between Pr and Ho as R. Only those with Sm, Eu, and Gd and  $x \simeq 0.9$  form bulk superconductors and then only when annealed at high  $\text{O}_2$  pressures. As shown in Fig. 15, one end of the  $T^*$ -phase unit cell resembles the  $\text{K}_2\text{NiF}_4$ -like structure of  $\text{La}_2\text{CuO}_{4-x}$  (called the T-phase), the first high- $T_c$  material to be discovered (by Bednorz and Müller). The other end of the unit cell resembles the structure of the so-called  $T'$  superconducting phase, Cc-doped  $\text{Nd}_2\text{CuO}_4$ . Each end has sites for the Sr, La, and R ions; the sites at the T-phase-like end are larger than those at the  $T'$ -like end. Consideration of the various atomic radii and the metal-oxygen distances for the two types of sites had led to the assumption that the larger ions ( $\text{Sr}^{2+}$  and  $\text{La}^{3+}$ ) occupy the larger T-phase sites, whereas the smaller rare-earth ions and the remaining  $\text{La}^{3+}$  occupy the smaller  $T'$ -phase sites. We examined the superconductor  $^{52}\text{La}_{0.99}\text{Sr}_{0.2}\text{CuO}_4$  with neutrons at LANSCE and with synchrotron radiation at the National Synchrotron Light Source at Brookhaven

National Laboratory. We tuned the synchrotrons radiation to absorption edges of La, Sm, and Sr to sufficiently modify their scattering factors. We also collected a fourth x-ray data set at a wavelength far from any edges. We found that the ordering exists but is incomplete: About 10% of the  $\text{Sm}^{3+}$  ions appear on the larger  $T$  site, presumably because the ions are nearly the same size, with a  $\text{Sm}^{3+}/\text{La}^{3+}$  ionic-radius ratio of 0.935. We also examined another superconductor,  $\text{La}_{0.9}\text{Gd}_{0.9}\text{Sr}_{0.2}\text{CuO}_4$ , in which the ions are of more disparate sizes ( $\text{Gd}^{3+}/\text{La}^{3+} = 0.91$ ). The strong absorption by  $^{64}$  precluded collection of a neutron powder pattern, but the four x-ray data sets were



sufficient to unambiguously determine the two site distributions for the three kinds of atoms. In this case the ions were well segregated into the two sites by their size. Since the two materials have similar superconductivity properties, this ordering evidently has little effect on the superconductivity.

## Conclusion

As one can see from this discussion, the science of powder diffraction has come a long way from its beginnings as a largely analytical tool. The Rietveld refinement technique has enabled the determination of crystal structures of considerable complexity and in fact was the first to accurately reveal the structures of the superconducting copper oxides. The power of this method can be further enhanced by proper combination of diffraction data from several radiation sources to improve the interatomic contrast and eliminate the ambiguities in powder structure refinements. ■

## $T^*$ -PHASE SUPERCONDUCTOR

Fig. 15. The structure of the  $T^*$ -phase superconductor (right) combines those of the  $T'$  and  $T$  phases, two other structures of  $\text{M}_2\text{CuO}_4$  (where M can be a lanthanide element or Sr in the compounds of interest for superconductivity). The  $T'$  phase (left) has Cc-doped Nd on the M sites (the parentheses around the "Cc" symbol indicate that the amount of Ce is much less than the amount of Nd). The  $T$  phase (middle) has larger sites for M, which are occupied by Sr-doped La. The  $T^*$  phase has La, Sr, and Gd on the M sites. The larger La and Sr ions occupy the sites in the top half of the unit cell, which are identical to those in the  $T$  phase. The smaller Gd (dark gray) ions and the rest of the La occupy the smaller  $T'$  sites in the bottom half.

## Crystal Symmetry Groups

Symmetry plays an important role in crystallography. The ways in which atoms and molecules are arranged within a unit cell and unit cells repeat within a crystal are governed by symmetry rules. In ordinary life our first perception of symmetry is what is known as *mirror symmetry*. Our bodies have, to a good approximation, mirror symmetry in which our right side is matched by our left as if a mirror passed along the central axis of our bodies. Our hands illustrate this most vividly; so much so that the image is carried over to crystallography when one speaks of a molecule as being either “right”- or “left”- handed. Those of us who live in an old-fashioned duplex will also recognize that such houses are built with mirror symmetry so that the arrangement of the rooms, hallways, and doors are disposed about an imaginary mirror passing through the common wall between the two halves of the house. There are many other examples of this kind of mirror symmetry in ordinary life. We can also see more complex symmetry in the patterns around us. It can be found in wallpaper patterns, floor-tile arrays, cloth designs, flowers, and mineral crystals. The basic mathematics of symmetry also applies to music, dance (particularly folk and square dance), and even the operations needed to solve Rubik’s cube.

The rules that govern symmetry are found in the mathematics of group theory. Group theory addresses the way in which a certain collection of mathematical “objects” are related to each other. For example, consider all the positive and negative integers and zero. They can constitute a group because under certain circumstances the relationships

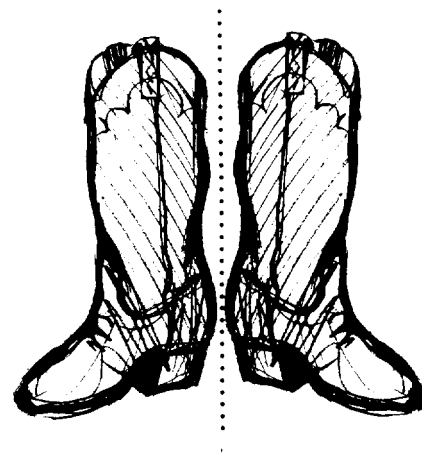
between the integers obey the rules of group theory:

- There must be defined a procedure for combining two elements of the group to form a third. For the integers one can choose the addition operation so that  $a + b = c$  is the operation to be performed and u, b, and c are always elements of the group.
- There exists an element of the group, called the *identity element* and denoted f, that combines with any other element to give the second one unchanged. In the case of the integers, the identity element is zero because any integer plus zero gives that integer ( $a + 0 = a$ ).
- For every element of the group, there exists another element that combines with the first to give the identity element; these are known as *inverse elements*. The negative integers constitute the inverses of the positive integers because their pairwise sums all equal zero, the identity element ( $a + (-a) = 0$ ).
- Group operations in sequence obey the associative law. For addition of integers this means that  $(a + b) + c = a + (b + c)$ . Notice that the commutative law,  $a + b = b + a$ , is not required even though it is true for this particular group.

You might be tempted to say that the positive integers, when related by multiplication ( $a \times b = c$ ), also constitute a group with the identity element now being one ( $a \times 1 = a$ ). In fact, the positive integers do not constitute a group under these conditions because, to obey the group-theory rules, the noninteger inverses ( $1/a$ ) as well as all the rational fractions ( $b/a$ ) would have to be included. The expanded set of positive

rational numbers *is* a group under multiplication, and both it and the integer group already discussed are examples of infinite groups because they each contain an infinite number of elements.

In the case of a symmetry group, an element is the operation needed to produce one object from another. For example, a mirror operation takes an object in one location and produces another of the opposite hand located such that the mirror doing the operation is equidistant between them (Fig. 1). These manipulations are usually called *symmetry operations*. They are combined by applying them to an object se-



### THE MIRROR SYMMETRY OPERATION

**Fig. 1. A pair of left- and right-“footed” boots illustrates the mirror-plane symmetry operation. The right boot can be positioned identically on the left boot by reflection through a mirror between them and vice versa.**

quentially. For example, doing a mirror operation twice on a right-handed object will, with the first operation, move it to the left-handed position, and with the second operation, place it back on its original right-handed position. In fact, applying a mirror operation twice in succession is equivalent to the identity

operation, so that a mirror operation is its own inverse.

The two operations, mirror and identity, obey the four rules of group theory, and thus constitute one of the simplest symmetry groups. A mathematical representation of these operations is

$$m^{-1} = m \text{ and} \\ mm^{-1} = mm = I.$$

Further, a "multiplication table" between these two operations can be set up to show the products that any pair of symmetry operations gives in this finite group (Fig. 2).

There are three types of symmetry operations in crystallography. The simplest type is the set of *translation operations* needed to fill a two-dimensional infinite plane or a three-dimensional infinite space. These operations form a group by themselves and have essentially the same characteristics as the example group of integers discussed above. The difference is that the translation group has two or three sets of integers depending on whether a two-dimensional plane or a three-dimensional space is filled. These translation operations make the concept of a unit cell possible, because once the unit cell for a crystal is specified, it takes only the right combination of translation operations to construct the full crystal lattice.

There is also a type of translation operation that relates objects *within* a unit cell so that the same objects are found at coordinates that are half multiples of unit-cell distances along two or three of the axes. These last operations are, for example, responsible for the face- and body-centered lattices found in three dimensions (Fig. 3). The possible combinations of this full set of translations for plane- and space-filling arrays (along with the restrictions on the rotation-symmetry operations that will

be discussed next) gives only five possible plane lattices and fourteen possible space lattices (Fig. 3).

The second type of crystallographic symmetry is *rotation*. For it to be a valid symmetry operation, however, the rotation angle  $\theta$  must be an integer divisor of 360 degrees, that is,  $\theta = 360/n$ , where  $n$  is an integer. The rotation-symmetry operations will then all be multiples of this rotation angle. For example, if  $n = 6$  the rotation angle is 60 degrees and the operations can be represented by the unique set  ${}^1C_6, {}^2C_6, {}^3C_6 (= {}^1C_2), {}^4C_6, {}^5C_6$ , and  ${}^6C_6 (= I)$  in which the subscript gives the fraction of

	<i>I</i>	<i>m</i>
<i>I</i>	<i>I</i>	<i>m</i>
<i>m</i>	<i>m</i>	<i>I</i>

## A FINITE SYMMETRY GROUP

**Fig. 2. This example of a simple, finite group obeying all the rules of group symmetry consists solely of the Identity element, *I*, and the mirror-plane symmetry operation *m*. The multiplication table shown above for the group gives the products for any pairwise application of the two symmetry operations.**

a full circle for each operation (here 1/6) and the superscript gives the multiple of 60 degrees used for the rotation (Fig. 4). Because  ${}^6C_6$  is the identity operation, these six rotation operations constitute a group, symbolized by C&

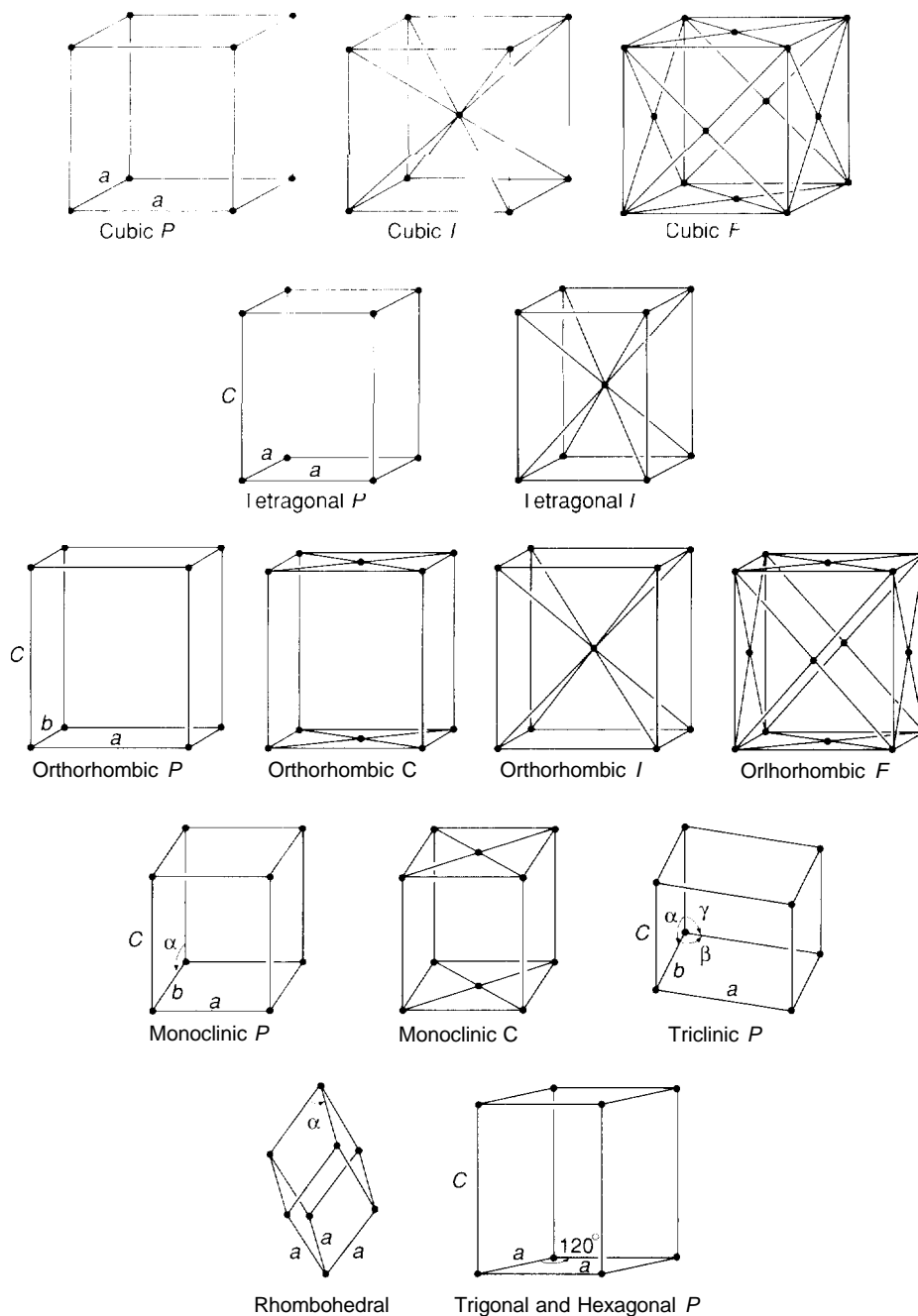
If the symmetry is local with no translation component, then the integer  $n$  can take on any value from one to infinity. An object that has the extreme case of  $C_\infty$  symmetry is a bowling pin, which an infinitesimally small rotation leaves looking the same (ignoring any painted design). However, when the rotation symmetry is part of a plane- or space-filling symmetry with translation operators, only five different rotation angles ( $n = 1, 2, 3, 4, \text{ or } 6$ ) can be used. Replication of a unit cell with a rotation symmetry other than these cannot fill a plane surface or three-dimensional space without leaving voids or having overlapping regions. The situation is more complicated in the three-dimensional case because a unit cell may also have different rotation symmetry in different directions. Many different groups result from the various combinations of these rotations.

An extension to the concept of rotation symmetry is to include in each rotation operator a translation component (Fig. 5). The resulting objects are helical or screwlike; hence, these operations are called *screw rotations*. These symmetry operations are most prevalent in crystal lattices in which the unit-cell repeat requirement means that the translation operations have the same integer fraction, or some simple multiple, as the rotation operations. For example, the screw rotation  $6_1$  describes an operation in which the rotation of 60 degrees is accompanied by a translation of 1/6 of the unit cell along the rotation axis. The  $6_2$  screw rotation has the same 60-degree rotation but this time is accompanied by a translation of 4/6 of the unit cell along the axis. A sufficient number of these is superimposed to give the required unit-cell translation (Fig. 5), and the resulting arrangement is different from that obtained with a  $6_1$  screw rotation.

The one facet common to the translation, rotation, and screw operations is

## THE BRAVAIS SPACE LATTICES

Fig. 3. The fourteen unit cells depicted above represent the only possible ways that space can be filled without gaps or overlaps between cells, that is, consonant with the restrictions of translation and rotation symmetry. The cubic cells at the top all have three orthogonal sides of equal length; the body-centered (*I*) and face-centered cubic cells (*F*) cannot be fully specified without also using translation operations in terms of half-cell distances. The tetragonal and orthorhombic cells also have sides that are mutually orthogonal, but either one side differs in length from the other two sides (tetragonal) or all three sides differ in length (orthorhombic). The monoclinic and triclinic cells have three unequal lengths but now either one angle (monoclinic) or all three angles (triclinic) between the sides do not equal 90 degrees. The rhombohedral cell can be thought of as a cubic cell that has been stretched or squeezed along a diagonal: the three sides are equal but the three angles, although equal, are not 90 degrees. The hexagonal cell has two angles of 90 degrees and one of 120 degrees; only two of its three sides are equal.

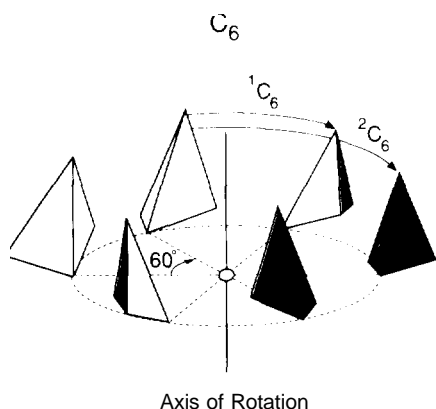


that none of these change the handedness of an object, and *changing handedness* is the major feature of the third type of crystallographic symmetry. We have already mentioned the mirror-symmetry operation that relates right- and left-handed objects across a plane. A similar operation is *inversion* (Fig. 6) in which right- and left-handed objects are arranged on opposite sides of a point, called an inversion center. The presence of an inversion center in a crystal is one of the primary classification features for crystal structures: such crystal structures are *centrosymmetric*. An example of the importance of inversion centers is that almost all biologically important molecules (proteins, amino acids, et cetera) do not have a self-contained inversion center and exist

in nature only in one-handed forms. Thus, they always crystallize in noncentrosymmetric crystal structures because the other-handed molecules do not exist.

In analogy to the operations combining rotations with translations to form

screw operations, mirror reflection can be combined with a fractional translation (always one-half of the unit cell) to form a new operation (Fig. 7). This is known as a *glide* operation, and the mirror part of the operation occurs at



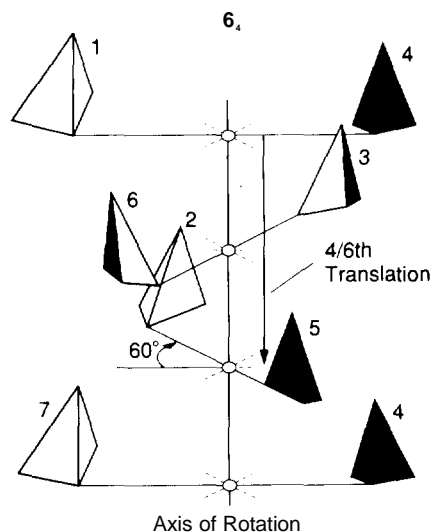
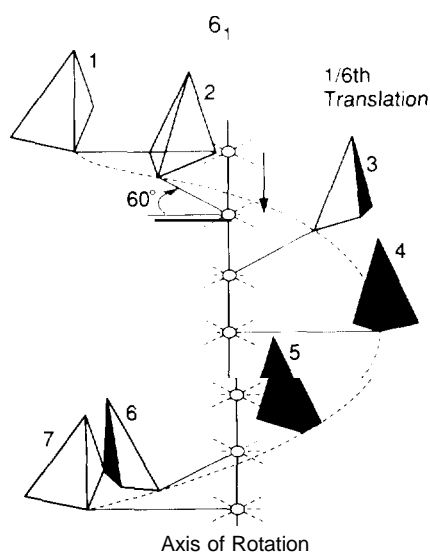
## ROTATION OPERATIONS

Fig. 4. The  $C_6$  rotation symmetry group consists of all the rotations about an axis that carry an object through angles that are multiples of 60 degrees. Two of the operations in the symmetry group,  ${}^1C_6$  and  ${}^2C_6$ , are labeled in the figure;  $C_6$  is the identity operation that carries the object a full 360 degrees back into itself.

a glide plane. Just as for the screw operation, glide operations are only found in crystal lattices where the repetition of translation and reflection can extend indefinitely. Similarly, an inversion operation can be combined with a rotation (Fig. 8). Because this operation occurs about a point, however, it is found in both isolated objects and in extended lattices,

When these operations are combined in ways that form two-dimensional planar arrays, only 17 unique plane groups are found. With three dimensions, the combination of operations gives just 92 centrosymmetric and 138 noncentrosymmetric space groups for a total of 230.

An additional type of operation worth considering is one that in a two-dimensional plane would, say, change the color of the object (see the opening figure of the main article). The simplest case is a "black-white" operator,



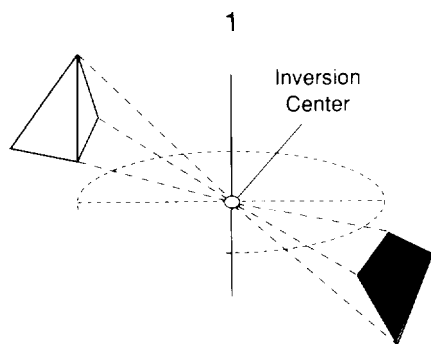
and such a color-reversal operator can also be combined with the other operators discussed earlier. An application of this type of operation is to describe the ordering of magnetic moments found in some materials by neutron scattering. Frequently, the moments arrange themselves in an alternating pattern so that every other one is "up" and all the others are "down." The symmetry of these arrangements can be described by including the color-reversal operation, which expands the total number

## SCREW ROTATIONS

Fig. 5. a) The  $6_1$  screw rotation is the application of a 60-degree rotation about a given axis of the unit cell followed by a translation along that axis of one-sixth of the unit-cell distance. This combination of symmetry operations is repeated successively along the full length of the unit cell (in the figure, the tetrahedrons generated by each successive combination of operations are numbered consecutively). Note that the placement of the tetrahedrons in this figure resembles the placement of the tetrahedrons for rotation alone (Fig. 4) except that the circle has been "stretched out" into an arc because of the vertical translation along the axis of rotation. After six rotation-translation operations, the tetrahedron has returned to its original orientation but is translated a full unit along one of the cell's axes. b) The  $6_4$  screw rotation is the same as the  $6_1$  screw rotation except the translation is now for four-sixths (two-thirds) of the unit distance. To fill in the whole pattern, the next rotation-translation operation (which ends up one-third of the way into the next unit distance) and successive operations are superimposed on the original unit distance. Note that in the figure the dashed line has been eliminated (because successive operations are superimposed), but the tetrahedrons generated by successive operations are still numbered consecutively. After three of these combined operations, the tetrahedron will have moved an integral number of unit distances (and thus can be pictured at either the bottom or top of the figure) but will have rotated only 180 degrees. In this manner, the tetrahedron ends up on both sides of the axis at each point along the way. Once again, after six combined operations the tetrahedron has assumed its original orientation.

of space groups to 1728 in 36 Bravais lattices.

Because there is an intimate relationship between the arrangement of atoms found in real space and the pattern of structure factors in reciprocal space,

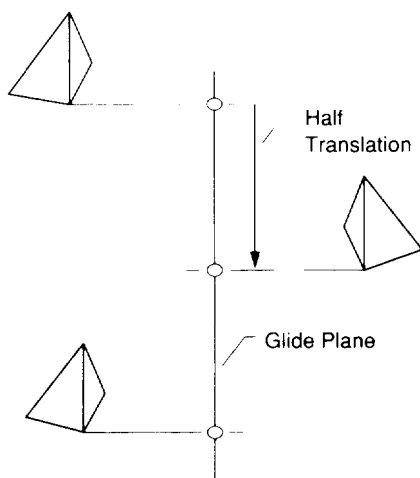


### INVERSION CENTER

**Fig. 6.** An inversion, denoted  $\bar{1}$ , is accomplished by “reflecting” everything through point or “inversion center” between the objects. The three dashed lines drawn between tips on the tetrahedrons and passing through the inversion center illustrate this operation.

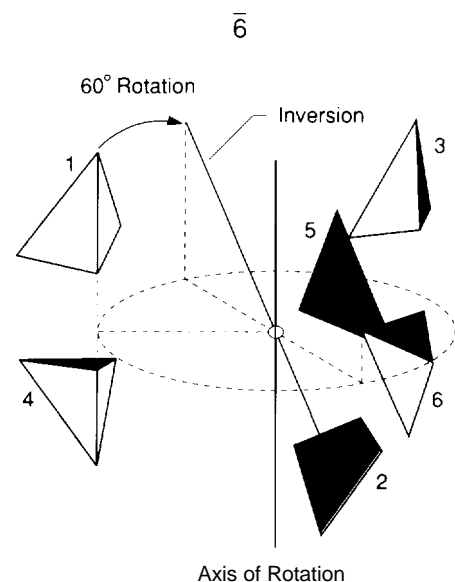
the symmetry of real space must have counterparts in reciprocal space. However, some of the symmetry aspects of reciprocal space may at first glance be surprising. Unlike crystallographic real space, which consists of a multitude of identical unit cells each with its own origin, reciprocal space has just a single origin and an infinite array of reciprocal-lattice points associated with differing and possibly complex numbers ( $F_h$ 's). Thus, none of the translational aspects of the crystallographic symmetry can show up in the reciprocal lattice other than in the dimensions of the reciprocal lattice itself. However, the rotation, mirror, and inversion symmetries present in the lattice are also present in the pattern of  $|F_h|^2$ 's on the reciprocal-lattice (that is, in the diffraction pattern). For example, the intensities and locations of the two-dimensional diffraction patterns shown in Figs. 4 and 5 in the main article have the same rotation and mirror symmetries as the two-dimensional patterns of scatterers that generated those patterns.

What of the other possible symmetry elements? A diffraction pattern almost always has a center of inversion—an inversion center is absent only for a noncentrosymmetric crystal containing an atom with a complex scattering factor. Half-cell translations and screw and glide-plane operations are revealed by *systematic extinctions*, that is, certain classes of reciprocal-lattice points with zero intensity. For example, in the diffraction pattern for a face-centered cubic lattice, the only points that have a nonzero intensity are those for which the  $hkl$  indices are all even (for example, 422) or all odd (for example, 311). Likewise, a glide operation whose glide plane is perpendicular to the  $c$  crystallographic axis and whose glide direction is parallel to the  $a$  axis causes the points with  $hk0$  indices and odd  $h$  to have zero intensity (for example, 120, whereas 210 has nonzero intensity). Systematic extinc-



### THE GLIDE OPERATION

**Fig. 7.** Here, mirror reflection and translation for one-half the unit distance are combined to form a glide operation. Note that the tetrahedron on the right side of the glide plane is the mirror image of the tetrahedrons on the left side; however, each tetrahedron is displaced a half unit from the last one.



### AN INVERSION-ROTATION OPERATION

**Fig. 8.** The  $\bar{6}$  symmetry operation is a combination of a 60-degree rotation followed by an inversion. Note that the three tetrahedrons above the plane are the same as the tetrahedrons in Fig. 4 for rotations of 0, 120, and 240 degrees (that is,  $I$ ,  ${}^3C_2$ , and  ${}^3C_2$ ). This happens because performing two successive  $\bar{6}$  operations is equivalent to performing the  ${}^3C_2$  operation (or two  ${}^3C_2$  operations). Lines showing the first combination of a 60-degree rotation and inversion operation are given on the figure as well as consecutive numbers for the successively generated tetrahedrons.

tions arise because the symmetry operation causes all the atoms to scatter with destructive interference for particular reciprocal-lattice points.

Thus, by examining both the symmetry of a diffraction pattern and the systematic extinctions, a crystallographer can usually identify one or two possible space groups for any crystal. However, some ambiguity may remain because of cases in which pairs of space groups display the same diffraction symmetry and systematic extinctions. ■



**Robert B. Von Dreele** has been a staff member at Los Alamos since 1986. (He had, however, established a connection with the Laboratory earlier by doing neutron powder diffractometry at the Omega West Reactor and by consulting at what is now LANSCE during the summers of 198&85.) His current responsibilities include the High Intensity Powder Diffractometer at LANSCE. He received his B.S. in Chemical Engineering and Ph.D. in Chemistry from Cornell University in 1966 and 1971, respectively. Immediately after completing his Ph.D. he joined the faculty of the Department of Chemistry at Arizona State University, where he remained until he joined the Laboratory. In 1971 he was a National Science Foundation Postdoctoral Fellow at Oxford University, where he worked on one of the first applications of the Rietveld refinement technique to neutron powder-diffraction data. A subsequent sabbatical year was spent as the first visitor to the "Neutron Beam Research Unit" (now ISIS) at the Rutherford-Appleton Laboratory in England. There he developed the first computer code capable of Rietveld refinement with time-of-flight powder-diffraction data from a spallation source. He later visited ISIS for seven months as a Fulbright Scholar.

## Further Reading

### Crystal Structures from X-Ray and Neutron Diffraction

- G. H. Stout and L. H. Jensen. 1968. *X-Ray Structure Determination: A Practical Guide*. New York: Macmillan Co.
- G. E. Bacon. 1975. *Neutron Diffraction*. Oxford: Clarendon Press.
- G. Harburn, C. A. Taylor, and T. R. Welberry. 1975. *Atlas of Optical Transforms*. Ithaca, New York: Cornell University Press
- D. L. Bish and J. E. Post, editors. 1989. *Modern Powder Diffraction*. Reviews in Mineralogy, volume 20, Washington, D.C.: Mineralogical Society of America.
- H. M. Rietveld. 1969. A profile refinement method for nuclear and magnetic structures. *Journal of Applied Crystallography* 2: 65.

R. A. Young, P. E. Mackie, and R. B. Von Dreele. 1977. Application of the pattern-fitting structure-refinement method to x-ray powder diffractometer patterns. *Journal of Applied Crystallography* 10: 262.

R. B. Von Dreele, J. D. Jorgensen, and C. G. Windsor. 1982. Rietveld refinement with spallation neutron powder diffraction data. *Journal of Applied Crystallography* 15:581.

### Crystallography And Crystal Symmetry

M. J. Buerger. 1963. *Elementary Crystallography*. New York: John Wiley & Sons.

J. E. Brigham, translator. 1972. *The Graphic Works of M. C. Escher*. London: Pan/Ballantine.

N. F. M. Henry and K. Lonsdale, editors. 1969. *Symmetry Groups*. International Tables for X-Ray Crystallography, volume 1. Birmingham: Kynoch Press.

M. Senechal and G. Fleck, editors. 1974. *Patterns of Symmetry*. Amherst, Massachusetts: University of Massachusetts Press.

G. Bums and A. M. Glazer. 1978. *Space Groups for Solid State Scientists*. New York: Academic Press.

B. K. Vainshtein. 1981. *Modern Crystallography. I. Symmetry of Crystals, Methods of Structural Crystallography* New York Springer-Verlag.

M. A. Jaswon and M. A. Rose. 1983. *Crystal Symmetry: Theory of Color Symmetry*. New York: Halsted Press.

T. Hahn, editor. 1985. *Space-Group Symmetry*. International Tables for Crystallography, volume A. Boston: Reidel.